Molecular mechanism of viral RNA recognition and MDA5 activation through LGP2

Duic Ivana

Table of contents:

ABSTRACT

The RIG-I-like receptor (RLR) proteins expressed in the cytoplasm of mammalian cells have the ability to recognize virus infections and initiate antiviral response. RLR proteins are activators of IFN-β in response to virus-derived RNA species. The RLR family is composed of three homologous proteins: RIG-I, MDA5 and LGP2. All of the family members share many structural features, in particular central DExD/H box RNA helicase domain that is homologous to the SF2 superfamily of RNA helicase proteins. All of them can recognize viral RNA and hydrolyze ATP, but each differs in enzymatic activity, ability to recognize RNA and mechanism of activation.

MDA5 and RIG-I form oligomeric complexes along dsRNA. Aligning their signaling domains, these proteins are able to propagate powerful antiviral response. LGP2 lacks signaling domain but participates in the viral sensing through cooperation with MDA5. This study utilized a biochemical and biophysical approaches to observe protein conformation and MDA5 fiber formation at high resolution. Experiments presented here revealed that LGP2 is incorporated into the MDA5/dsRNA complex enhancing the MDA5 fiber dynamics through ATP hydrolysis. Furthermore, limited protease digestion indicated that LGP2 promotes MDA5 CARDs exposure. These data demonstrated the coordinated actions of MDA5 and LGP2 where LGP2 acts as MDA5 nucleator and requisite partner in the mechanism of MDA5 activation, revealing a mechanistic basis for the LGP2 mediated regulation of the innate immune response.

ABBREVIATIONS

AcTeV	enhanced form of Tobacco Etch Virus protease
ADAR	double stranded RNA-specific adenosine deaminase
AFM	Atomic Force Microscopy
AGS	Aicardi-Goutieres syndrome
AMP-PNP	adenylyl-imidodiphosphate
ATP	adenosine triphosphate
BPEV	Bell pepper Endornavirus
CARD	caspase activation and recruitment domain
CBB	Coomassie Brilliant Blue
CTD	carboxy terminal domain
dsRNA	double stranded RNA
EMCV	encephalomyocarditis virus
GST	gluthatione S-transferase
HCV	Hepatitis C Virus
Hel2i	specialized helicase insertion domain that facilitates RNA recognition
HEPES	4-(2-hydroxyethyl)-1-piperazineethanesulfonic acid
HRP	the enzyme horseradish peroxidase
HS-AFM	high-speed atomic force microscopy
IFN-β	interferon beta
IKK	inhibitor of nuclear factor kappa-B kinase
IRF3	interferon regulatory factor 3
ISG	interferon-stimulated genes
LGP2	laboratory of genetics and physiology 2
MDA5	melanoma differentiation associated gene 5
MAVS	mitochondrial antiviral signaling protein
mRNA	messenger RNA
NDV	Newcastle disease virus
NFκB	nuclear factor kappa B
PAGE	polyacrylamide gel electrophoresis
PAMP	pathogen-associated molecular pattern

Poly(I:C)	polynosinic:polycytidylic acid; dsRNA synthetic analog
PRR	pattern recognition receptor
PVDF	polyvinylidene fluoride
RIG-I	retinoic acid inducible gene
RLRs	rig-i-like receptors
SDS	sodium dodecyl sulfate
SEV	Sendai Virus
SLE	systemic lupus erythematosus
SPM	Scanning Probe Microscope
ssRNA	single stranded RNA
T1D	type 1 diabetes
TBK1	TANK binding kinase 1
TNF	tumor necrosis factor
TRAF	TNF receptor associated factor
VSV	Vesicular Stomatitis Virus

Chapter 1

Introduction

INTRODUCTION

1.1 RLRs background

The innate immune system is the front line of defense of a host cell against pathogenic invasion. In the cytoplasm, several sensor proteins function against viral invasion. Retinoic acid inducible gene I (RIG-I), a DExD/H box RNA helicase, is identified as the cytoplasmic PRR (pattern recognition receptor), sensor for viral RNA, which triggers a signaling pathway resulting in type I interferon induction [1, 2]. Melanoma differentiation-associated gene 5 (MDA5), laboratory of genetics and physiology 2 (LGP2), along with RIG-I, are collectively known as the RIG-I like receptors (RLRs). RIG-I and MDA5 have two copies of Caspase Recruitment Domain (CARD) at its N terminus, responsible for signaling, a helicase domain and a C-terminal domain, responsible for viral RNA recognition. LGP2 lacks CARD domain, therefore it is unable to activate signaling by itself, but participates in the viral sensing through cooperation with RIG-I and MDA5. Analyses using RLR gene knockout mice revealed that these receptors are playing an important role in recognition of various types of RNA viruses and triggering antiviral innate immune responses [3, 4].

Although they share highly homologous structure (Illustration 1), RLR proteins differ in their RNA recognition and signaling capability. Several lines of evidence indicate that RNA recognition by RIG-I and MDA5 occur with CARD dephosphorylation [5], which enables their interaction and further signaling. RLR signaling pathway was developed mostly by studying RIG-I. Interaction with non-self RNA leads to the conformational change and activation of CARDs which enables these proteins to associate with CARDs of mitochondrial antiviral signaling protein MAVS [6]. MAVS acts as a signaling stage that facilitates activation of signaling proteins TRAF2, TRAF5,

TRAF6, including serine kinases IκB, IKKα, IKKβ, IKKγ, IKKε and TBK1 [7]. This activates the transcription regulators, IRF3 and NFκB that induce the production of IFN-β. Secreted INF-β induces the expression of other effectors, all together producing an effective cellular defense against virus replication (Illustration 2).

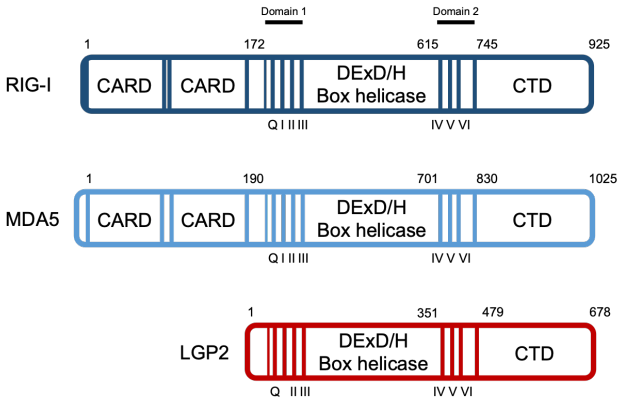

Illustration 1: RLRs structure

RIG-I and MDA5 sense distinct set of viral infections. The virus specificity likely originates from different structures of viral RNA generated in the infected cells. Subsequent experiments revealed that dsRNA commonly activates both, RIG-I and MDA-5, however, there are some critical determinants in ligand selectivity of RIG-I and MDA5. RIG-I responds to short, long, ssRNA, viral hairpins, tri- or diphosphate RNA ends, and HCV poly(U)-rich untranslated region. RIG-I deficiency in mice results in high susceptibility to viral infections such as Newcastle disease virus, vesicular stomatitis virus, Sendai virus and influenza A virus [4, 8]. RNA recognition by RIG-I involves its conformational changes and ATP-powered translocations along dsRNA [9].

The mechanism of viral RNA recognition by MDA5 and LGP2 remains more enigmatic. Specific characteristics of MDA5 ligand are still unknown, partially due to its poor RNA binding affinity. However, several studies revealed some of potential RNA features discriminated by MDA5 such as: RNAs longer than 2 k bp, structural features such as RNA branches, features specific to virus-derived mRNAs, including primary and secondary structures, and also those RNAs that successfully escape RIG-I by masking their 5’ ends. One of them is EMCV RNA. This virus replicates more efficiently in the absence of MDA5 or LGP2. A region of EMCV negative-strand RNA

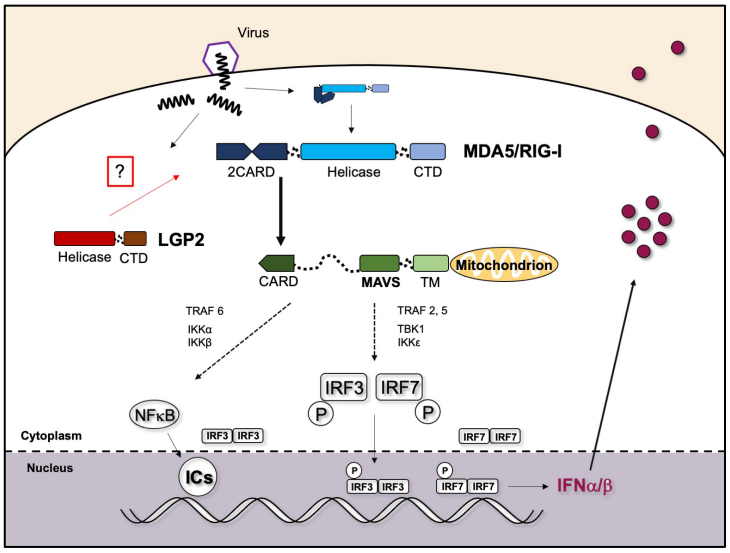

Illustration 2: RLRs antiviral signaling pathway

was found to co-purify with LGP2 [10]. This RNA is necessary for antiviral response mediated by MDA5. While this fails to reveal some specific feature required for MDA5 recognition, it contributes to the growing evidence of MDA5 and LGP2 collaboration in antiviral response. Moreover, proteins encoded by paramyxoviruses target MDA5 and LGP2 to disrupt their ATP hydrolysis and inhibit activation of the immune response [11]. This suggests the importance of both: MDA5-LGP2 synergy, as well as ATP hydrolysis.

LGP2 lacks CARD domain or any other known signaling domain (Illustration 1), therefore it is hard to fully understand its role in antiviral signaling. LGP2 is present at low levels in uninfected cells but accumulates in response to virus infection [12]. It has the highest RNA binding affinity of all RLRs, and it has no specific preferences. It has ability to recognize diversity of RNAs, irrespective of their length or 5' phosphate ends. Based on these findings, LGP2 was originally suggested to sequester viral RNA from detection by RIG-I [13]. However, LGP2 proteins defective for RNA binding can still inhibit RLR signaling, indicating that RNA competition cannot explain this effect of LGP2 [14]. On the contrary, mice lacking LGP2 exhibited decreased IFN-β production in response to RNA viruses [15]. The role of LGP2 in immune responses is controversial due to different reports of LGP2 as both, positive and negative regulator. LGP2 also appears to act as a concentration-depended biphasic switch. It enhances MDA5 mediated signaling only when it is present at relatively low concentrations. At very high

levels, LGP2 will inhibit MDA5 function [15, 16, 17]. However, LGP2 appears to have an important role in fully functional and rapid activation of IFN response during early stages of infection.

1.2 RLRs activation and conformational changes

RIG-I is present in the cytoplasm in auto-inhibited state [18]. It is activated only by the CTD binding to the appropriate ligand. In the ligand free environment, the two CARDs are interacting with the Hel2i insertion domain, while CARDs are unavailable for downstream signaling, CTD retains flexibility to scan the cellular environment for foreign RNAs. When CTD recognizes appropriate ligand, conformational change is initiated, and dsRNA helix displaces the CARDs. This allows helicase domains to form a ring-like structures around RNA and CARDs are free for downstream signaling and interaction with MAVS [19, 20]. The CARDs are also regulated and modified *in vivo* by CARD ubiquitination, phosphorylation and via interaction with other regulatory proteins [21]. After this initial transformation into enzymatically active form, RIG-I is utilizing ATP hydrolysis to translocate along the dsRNA [9]. The presence of CARD domains inhibits this translocation, however when dsRNA contained 5'-ppp modification, CARD did no longer have inhibitory effect [22]. In the absence of ATP, RIG-I binds to RNA ends as a monomer, but in the presence of ATP it assembles into a fiber starting at the dsRNA end and elongating toward the interior. These fibers do not entirely cover RNA, but they are rather observed as multiple short fibers at the end of RNA and sometimes internally along RNA [23].

Naïve MDA5 is incompetent for signaling. The mechanism by which MDA5 CARDs are sequestered in the naïve state is so far unknown. As mentioned above, it

is difficult to identify key features of ligands required for MDA5 recognition. This is most likely related to structural differences between MDA5 and RIG-I, as well as low RNA binding affinity. CTD of RIG-I contains 5'-ppp or 5'-pp binding pockets, the analogous surface on the CTD of MDA5 is flatter and has much lower affinity for dsRNA. The CTD of MDA5 is involved in cooperative binding. Therefore, MDA5 is able to form fibers on dsRNA, with ring-like asymmetric units that form helical twists [24]. Initially it binds slowly as a monomer or dimer and form long head-to-tail fibers at any location along dsRNA. Physiological levels of ATP promote MDA5 dissociation from RNA [25], but it is still unclear if dissociation is a positive or a negative mechanism of signaling regulation. Additionally, MDA5 fibers were never observed in living cells, suggesting this is an extremely dynamic process and a short stage in antiviral signaling, rather than an intracellular structure.

LGP2 possess the strongest RNA binding affinity of all RLRs, and as mentioned above, that was interpreted as evidence for RNA sequestration as an inhibitory mechanism [26]. However, this negative regulatory activity of LGP2 remains intact in the absence of RNA binding ability or ATP hydrolysis activity [14, 16]. LGP2 is the only RLR that possess dual ATPase activity, basal and RNA stimulated ATPase activity. The exact mechanism how LGP2 binds diverse RNAs, how it can enhance MDA5 signaling and inhibit RIG-I, remain unknown.

1.3 The role of ATP in RLRs signaling

ATP binding and hydrolysis by the helicase domain appears to be of great importance for antiviral function of RLRs. Previous reports failed to detect ATP depended dsRNA strands unwinding by MDA5 or LGP2, suggesting uncertainty regarding these proteins functioning as a real RNA modifying proteins [27]. These observations raise the question about the exact role of ATP in RLRs signaling. The energy released from ATP hydrolysis could be used in several ways and this remains a debate for many years. Recent studies suggest that the ATPase activity of SF2 helps to increase the selectivity of viral RNA or decrease the affinity for self-RNA [28-32]. At first, MDA5 signaling seemed to be independent of ATP because both, ATP binding and hydrolysis-deficient mutants were found to induce a constitutive immune response [29].

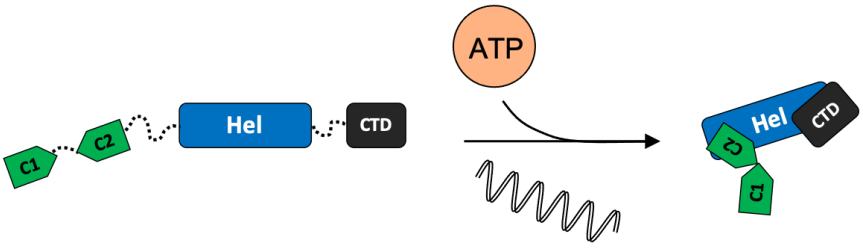

Illustration 3: MDA5 RNA+ATP induced conformational change

However, *in vitro* assembled MDA5 fibers were shown to dissociate in the presence of ATP, presumably due to conformational changes induced by cycles of ATP binding and hydrolysis [33]. Destabilization of fibers due to ATP hydrolysis is stronger at ends because MDA5 is less stable there leading to more rapid fiber disassembly [29]. MDA5 defective for ATP hydrolysis has been implicated in autoimmune and autoinflammatory diseases such as systemic lupus erythematosus (SLE), Aicardi–Goutières syndrome (AGS) or type 1 diabetes (T1D) [34, 35]. These findings suggest that ATP binding and hydrolysis have important role in the regulation of MDA5 signaling.

In the case of RIG-I consent is reached with respect to the role of ATP binding, whereas the role of ATP hydrolysis again remains a debate. dsRNA and ATP binding are required to trigger the conformational change that liberates CARDs from Hel2i [29-31]. Several groups utilized non-hydrolysable ATP analogues to investigate the purpose of ATP hydrolysis. In addition, mutation in motif II allows ATP binding but prevents or slows down hydrolysis, trapping the protein in ATP-bound state. Interestingly, this site in motif II was found to be mutated in atypical Singleton-Merten syndrome as well and was suggested to lead to an autoactivated state of RIG-I in uninfected cells [36]. Subsequent cell-based studies with RIG-I trapped in ATP-bound state suggested increased interactions with self-RNAs that lead to an autoactivated state of RIG-I even in the absence of an infection [29, 31]. However, in some studies this motif did not lead to an increased RIG-I signaling [14, 32]. One explanation of these differences is different cellular background in which the studies were conducted.

LGP2 is the most mysterious protein in RLR family. As mentioned above, it possesses dual ATPase activity. High basal ATPase activity enhances LGP2 ability to recognize diverse RNAs [16]. If this ability is involved in the regulation of MDA5 or RIG-I remains to be investigated. So far, there are no reported autoactivation diseases in direct connection with LGP2. However, growing evidence suggested that LGP2 has been also linked to tissue-specific functions in adaptive immunity responses, cancer and apoptosis [37, 38, 39]. From this one can postulate that LGP2 has a much more important role than it has been previously thought.

In summary, ATP binding and hydrolysis are one of the central features critical for accurate RLRs signaling. ATPase may play a regulatory role different for each signaling receptor and their signaling context. It can be speculated that RLRs utilize ATP for one: enhancement of RNA selectivity, two: proofreading and displacement

from non-optimal pathogen-associated molecular patterns (PAMPs), or three: increasing the signaling by promoting turnover of multiple molecules on single dsRNA. Perhaps, all these three options are utilized and balanced to achieve the most efficient signaling against pathogens and, at the same time, prevent self-RNA recognition.

1.4 RLRs in autoimmune disorders

IFNs are protecting us against viral infections but can also be damaging and are associated with the development of autoimmune disorders. Therefore, dissecting the mechanism by which immune receptors mediate induction of IFN and ISGs is of great importance. IFN signaling is associated with several autoimmune disorders, such as systemic lupus erythematosus, rheumatoid arthritis, systemic sclerosis, type I diabetes, Graves' disease and psoriasis [40-46]. These diseases are characterized by sever inflammation and autoimmunity that have been a consequence of IFN induction, however, the precise mechanism is still unknown. Suppressing IFN signaling in these conditions is thought to have a clinical benefit, but this approach has risks. Immune regulation by IFNs is very complex and blocking it might be detrimental. Entirely blocking IFN pathway would cause these individuals to be extremely vulnerable to viral infections [47-50]. This can be avoided by targeted therapeutic approach. Therefore, better understanding of the mechanism and individual contributors to the immune response is crucial.

As mentioned above, RLRs and their ATPase activity have been implicated in autoimmune disorders. All three members of the RLR family have overlapping but distinct affinity for different RNAs and these RNAs are characteristic of viral replicative

intermediates. However, these RNAs are also produced endogenously, especially duplex RNA. Very tight regulation to prevent autoactivation of the helicases must exist.

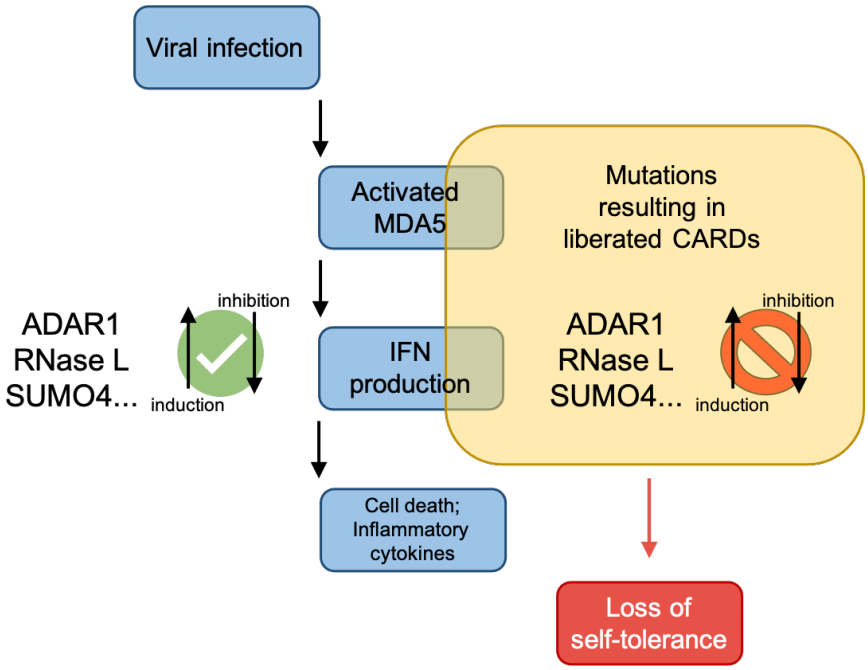

Illustration 4: Multiple errors in MDA5 signaling pathway that can lead to the loss of self-tolerance and autoimmunity

In view of the RLRs, there are several points that could be disrupted resulting in autoactivation. For example, IFN signaling, which induces the expression of MDA5, also induces the RNA-specific adenosine deaminase (ADAR1), which edits endogenous RNAs and in that way, prevents activation of the MDA5. Loss-of-function mutations in ADAR1 have been identified to cause AGS [51]. Furthermore, the fatality of ADAR1 deficiency also depends on another IFN-regulated gene – RNase L [52]. RNase L is activated by 2'-5'-oligoadenylate synthase-1 and produce RNA that activates MDA5 [53]. Interestingly, gain-of-function mutations in 2'-5'-oligoadenylate synthase-1 have been identified in T1D patients [54]. Also, MDA5 mis-sense mutations are associated with autoimmunity in mice, caused by constitutive activation of the IFN pathway [55]. Whether the prevention of self-RNA recognition, regulation of the MDA5

conformation, or both mechanisms are involved in autoimmunity, needs to be investigated. However, the role of MDA5 activity in autoimmunity is evident.

The activity of RIG-I and MDA5 is also regulated by posttranslational modifications. Ubiquitin and ubiquitin-like molecules play an important role in this pathway. Lysine 63-linked polyubiquitination is essential for MDA5 and RIG-I activity [56-59]. Lysine 48-linked ubiquitination of RIG-I, MDA5, and the adaptor MAVS regulates their degradation [60]. RLRs induce IFN and are themselves induced by IFN. The fine balance of this induction and degradation is critical in the context of autoimmune disease. Taken all together, autoimmunity is a multifunctional disorder, result of genetic and environmental triggers and multiple “checkpoints” need to be in perfect balance to prevent the disease (Illustration 4).

1.5 Study implications

LGP2 plays a role in variety of contexts and differences in cellular concentration or type of a ligand yield different outcomes. This is interesting in the case of MDA5, because it is known that LGP2 deficiency results in decreased IFN-β production in response to viruses usually recognized by MDA5. While it was known that LGP2 can enhance MDA5 signaling, it was not clear by which mechanism. It has been proposed that MDA5 binds to long dsRNA by forming fiber-like polymers where the tandem CARD signaling domain is exposed, thereby becoming capable of triggering antiviral signaling. This study reveals that LGP2 accelerates MDA5 fiber formation and adoption of its activated conformation. In the presence of ATP, LGP2 facilitates dissociation of the fibers. However, dissociated MDA5 preserves its activated conformation. This could mean that MDA5 has a 'memory' of encountering a viral RNA even when it is dissociated from the RNA.

Findings presented here indicate that LGP2 is able to affect MDA5 activation, and this could provide a basis for further advance in our understanding of the LGP2 role in innate immunity. Moreover, these findings could give us some clues about the mechanism of autoimmune disorders linked with MDA5 mutations. This study suggests a new model of the dsRNA recognition by MDA5/LGP2 and expansion of antiviral signaling in the cytoplasm.

Chapter 2

Materials and Methods

MATERIALS AND METHODS

2.1 Cell culture and plasmids

HEK293T cells were cultured in Dulbecco's modified Eagle's Medium (DMEM) with 10% fetal bovine serum (FBS) and penicillin/streptomycin (100 U/ml and 100 μg/ml respectively; Nacalai Tesque, Japan).

The p-125 Luc and p-RL-tk have been described previously [1]. pEF-BOS-FLAG-MDA5 and pEF-BOS-FLAG-LGP2 were obtained by subcloning cDNA into the empty pEF-BOS vector with the oligonucleotides for the N-terminal FLAG-tag. Mutants were generated by introducing the mutations into pEF-BOS-FLAG-MDA5 or pEF-BOS-FLAG-LGP2 using the KOD-Plus-Mutagenesis Kit (TOYOBO).

2.2 Preparation of BPEVdsRNA

Long dsRNA is difficult to prepare by conventional methods, therefore natural RNA was used. Long dsRNA from green pepper, which is a genome of Endorna virus, was identified and a protocol for its large-scale preparation was established. The family *Endornaviridae* infects diverse hosts including plants, fungi and oomycetes. The virus is transmitted through seeds and spores. It has no harmful effect on the host. Bell pepper (a group of the species *Capiscum annuum*) poses this virus originated double strand RNA with a length of 14 k bp. This dsRNA was extracted and purified for further experiments as a mimic model of viral RNA (a). The green bell peppers (*Kyosozu* and *Miogi* strains) were crushed using low-speed compression juicer. The juice was fractionated into four fractions: nuclear, organelle, vesicular and cytosolic fraction. The

RNA from the organelle fraction was extracted by phenol-chloroform. The sample was treated with DNase 1 (Roche), followed by total RNA phenol extraction and ethanol precipitation. This RNA was subjected to agarose gel electrophoresis and recovered by GENECLEAN II Kit (MP Biomedicals) (b). The quality and purity of the dsRNA was confirmed by agarose gel electrophoresis and AFM (c).

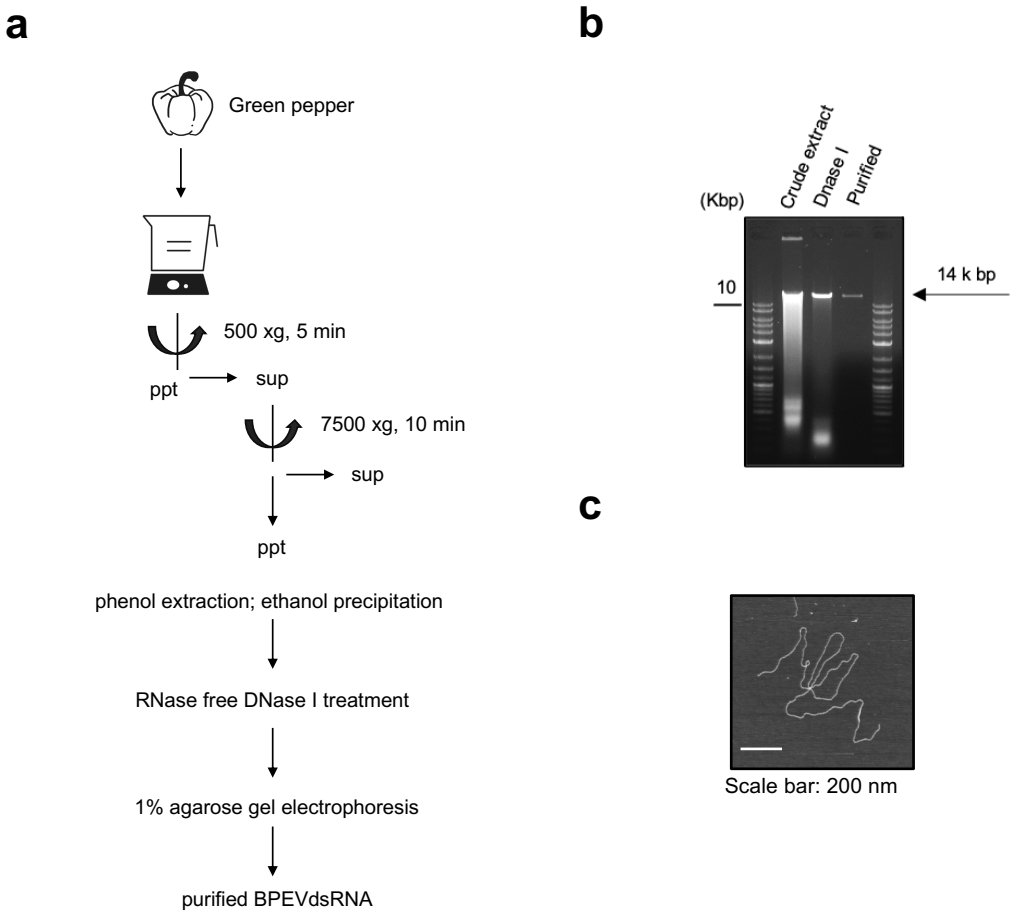

2.3 Luciferase assay

HEK293T cells were seeded into 12-well plate ($0.1x10^6$) the day before transfection. Cells were co-transfected with p-125 Luc, p-RL-tk, pEF-BOS-MDA5 with addition of pEF-BOS-LGP2 or mutants using linear polyethyleneimine (PEI) under standard conditions. After 24 hours cells were further transfected with poly (I:C), BPEVdsRNA using PEI or infected by EMCV. Luciferase activity was determined using the Dual-Luciferase Reporter Assay System according to the manufacturer's instructions (Promega). Reporter gene activity was normalized to the internal control.

2.4 Recombinant RLR proteins purification

GST-Flag MDA5 was produced using Bac-to-Bac Baculovirus Expression System (Invitrogen, Life Technologies). The protein was expressed as GST fusion protein in High Five insect cells and purified using Gluthatione Sepharose 4B (GE Healthcare). GST tag was removed by AcTeV protease (Invitrogen). Coexisting nucleic acids were removed by Q Sepharose HP (GE Healthcare). Final protein conformation was examined by AFM.

6xHis-Flag LGP2 was produced using Baculovirus Expression System. The protein was expressed as N-terminal 6xHis tag fusion protein in High Five insect cells. 6xHis-LGP2 was bound to Ni Sepharose 6 Fast Flow (GE Healthcare) and eluted in elution buffer containing 50 mM Tris-HCl (pH 8.0), 150 mM NaCl, 1.5 mM DTT and 500 mM imidazole.

2.5 ATPase assay

Protein (2 μg) and GP dsRNA (500 ng) mixtures were incubated at room temperature for 10 minutes in buffer: 20 mM Tris-HCl pH 7.5, 1.5 mM $MgCl_2$, 1.5 mM DTT, in 20 μl. Where indicated LGP2 or LGP2 K30G was added (200 or 400 ng). After adding 1 mM ATP, mixture was incubated at 37°C for 30 minutes. Presence of released free phosphate was detected by BiomolGreen (Enzo Life Sciences). Absorbance was measured in microplate reader 680 in a range of 630-850 nm (BIO RAD).

2.6 Size Exclusion Chromatography – Sepharose 4B

SEC was used to detect protein size shifts. The 2.4 ml column was assembled using glass Pasteur pipette with short capillary tip and cotton ball at the bottom. Columns were sterilized and filled with Sepharose 4B (GE Healthcare). Prior to adding the sample, the column was washed and equilibrated with 5 ml (in total) of buffer B (50 mM Tris, 150 mM NaCl, 1.5 mM DTT, 5 mM $MgCl_2$). Typically, samples contained 3.4 μM MDA5, 125 nM dsRNA, 5 mM ATP. After the sample was loaded, 100 μl fractions were collected. Fractions were than analyzed by immunoblotting using anti-Flag antibody or condensed by precipitation by acetone before immunoblotting in the case where the sample was fractionated twice.

2.7 MDA5/Poly (I:C) complex formation and fractionation

Recombinant MDA5 (3.4 μM) and poly(I:C) (30 μg) were incubated in the buffer B. SEC (Sepharose 4B) was used to isolate the complex. Fractions 8, 9 and 10 containing MDA5/poly(I:C) complexes were pooled and treated with 5 mM ATP or 5 mM ATP + 2.5 μM LGP2. Samples were incubated at 37°C for 30 min and then ultra-centrifuged at 300,000 x g for 10 min (Beckman Coulter, Optima MAX-XP, TLA 120.2). Samples were mixed with native sample buffer (0.25 M Tris-HCl, pH 6.8, 40% glycerol, 0.005% bromophenol blue) and then subjected to 6% Native-PAGE (without SDS). Buffer for anode chamber: 25 mM Tris-HCl, pH 6.8, 192 mM glycine, and cathode chamber: same buffer supplemented with 1% DOC. The gel was pre-run for 60 min at 40 mA, the samples were electrophorized for 6 h with constant 60 V at 4°C. MDA5 was visualized by immunoblotting (anti-MDA5-CTD antibody).

2.8 Tryptic digestion of proteins and protein/RNA complexes

MDA5 or MDA/LGP2 alone or complexed with poly (I:C) (at 1:1 mass ratio) in the absence or presence of 2 mM AMP-PNP or 2 mM ATP as a 25 μg samples were treated with 0.035 μg of Trypsin from bovine pancreas (TPCK treated: Sigma-Aldrich). At the indicated time intervals 10 μl samples were removed and reaction was stopped by the addition of SDS-sample buffer and heating at 95°C for 5 min. Samples were subjected to SDS-PAGE and silver stained with Sil-Best Stain One (Nacalai Tesque, Japan) following manufacturer's instructions.

2.9 Peptide sequencing

Digested MDA5 (as described in 2.8) was subjected to 7.5% SDS-PAGE and transferred to a PVDF membrane, followed by 0.1% CBB R-250 staining. Membrane was dried and band was excised using a sterile razor. N-terminal amino acid sequence of trypsin-digested MDA5 was determined by Japan Institute of Leather Research.

2.10 Antibodies and antibody labeling

Anti-Flag and anti-GFP were purchased from Sigma and Santa Cruz Biotechnology, respectively. The anti-human LGP2 antibody was originally generated by immunizing rabbits with a synthetic peptide corresponding to amino acids 535-553 of the human LGP2, as described previously [61].

Antibody labeling: anti-LGP2 and anti-GFP were labeled with Qdot 655 nanocrystals using SiteClick™ Qdot™ 655 Antibody Labeling Kit following manufacturer's instructions (Invitrogen, Thermo Fischer Scientific, USA).

2.11 AFM sample preparation

Purified recombinant proteins and BPEVdsRNA were diluted in buffer C (5 mM HEPES-NaOH pH 7.5, 50 mM NaCl, 5 mM $MgCl_2$, 150 nM MDA5, 8.4 nM dsRNA, 30 nM LGP2). Mixtures were incubated at the times indicated with or without 1 mM ATP at 37°C. RNA/protein samples were fixed with 0.05% glutaraldehyde (Nacalai tesque, Japan), placed on freshly cleaved 10 mM Spermidine treated mica for adhesion, and dried with nitrogen gas prior to imaging.

2.12 AFM imaging

AFM imaging was performed using Multimode AFM Nanoscope® IIIa controller and a J scanner (Bruker, Veeco, Digital Instruments). The AFM machine was operated in Tapping Mode at a scanning rate of 1-2 Hz in air at room temperature using silicon rectangular micro cantilevers with sharpened tetrahedral tips (OMCL-AC160TS-C3, Olympus Corporation, Tokyo, Japan). The cantilevers had a spring constant of 26 N/m and a resonance frequency of 300 (±100) kHz. Images were taken from height data and flattened in the NanoScope Analysis (v. 5.31 rl, Digital Instruments).

2.13 AFM image analysis

The flattened SPM images were analyzed with NanoScope Analysis (v. 5.31 rl, Digital Instruments and 1.40, Bruker). Section analyses were done in the software drawing a line at the point of interest and converting a corresponding curve graph data into a text file.

2.14 High-Speed AFM

Imaging of the dynamics of MDA5 molecules were performed using a high-speed AFM system (Nano Live Vision, Research Institute of Biomolecules Metrology Co., Tsukuba, Japan) with a custom-made piezo scanner, the resonance frequencies of which are xy 30 kHz and z 600 kHz. Small silicon nitride cantilevers were used (BL-AC10EGS-A2 cantilevers; Olympus Co., Tokyo, Japan). Their resonant frequencies in water were

~ 600 kHz, and the spring constants in water were ~ 0.1 N/m. Each cantilever had an electron beam deposited (EBD) probe.

A 2 μL droplet of MDA5 solution (0.5 ng/μL) was deposited onto the surface of freshly cleaved mica (1.5 mm diameter). After incubation for 1 min at room temperature, the sample was gently rinsed several times with buffer C (20 mM Tris-HCl (pH 7.5), 10 mM $MgCl_2$, and 1 mM EDTA) to remove unabsorbed molecules. High-speed AFM imaging in tapping mode was performed in the same buffer solution. The 192 × 144 pixel images were obtained at a scan rate of 2.0-5.0 frame/s and analyzed with the ImageJ software (National Institue of Health (NIH), Bethesda, MD, USA, http://rsbweb.nih.gov/ij/).

Chapter 3

Results

RESULTS

3.1 LGP2 and MDA5 co-expression enhance IFN-β promoter activity in response to Poly (I:C), EMCV and BPEVdsRNA

To investigate LGP2 effect on MDA5 IFN-β induction upon stimulation by different RNA species synthetic RNA (Poly (I:C)), virus (EMCV) and natural RNA (BPEVdsRNA) were used. Long dsRNA is difficult to prepare by conventional methods. 14 k bp long dsRNA from bell pepper (*Capiscum annuum*), which is a genome of Endornavirus, was identified and a protocol for its large-scale preparation was established [62]. This BPEVdsRNA was extracted and purified for further experiments as a mimic model of viral RNA. Experimental design is shown (Fig. 1A).

Overexpression of MDA5 induced the basal promoter activity; however, it was further upregulated upon Poly (I:C) transfection in HEK293T cells. Addition of low concentration of LGP2 significantly enhanced IFN-β induction (Fig. 1B). This data is consistent with the previous reports [16, 63]. Upon EMCV infection, IFN-β is induced when MDA5 and LGP2 are co-expressed, while the level of IFN-β induction was comparable to that of uninfected cells when MDA5 was expressed alone (Fig. 1C). Similar effect was observed when cells were transfected with BPEVdsRNA (Fig. 1D). When mutants of LGP2 (ΔCTD: helicase only, CTD: CTD only) were co-expressed with MDA5, no cooperation was observed (Fig. 1B-D), suggesting that full length LGP2 is required to cooperate with MDA5. LGP2 K30G, whose ATP binding site is disrupted, exhibited significantly reduced cooperation with MDA5.

MDA5/LGP2 co-expression increased the level of IFN-β induction compared to the cells expressing MDA5 alone in response to synthetic, viral or natural mimic of

a viral RNA. Since LGP2 lacks a signaling domain, as expected, LGP2 overexpression alone did not induce IFN-β compared to the mock (Fig. 1B-D). Thus, these results suggested MDA5/LGP2 cooperation in response to various long dsRNA species and the necessity of the full length LGP2 for this phenomenon, as well as functional ATP binding site.

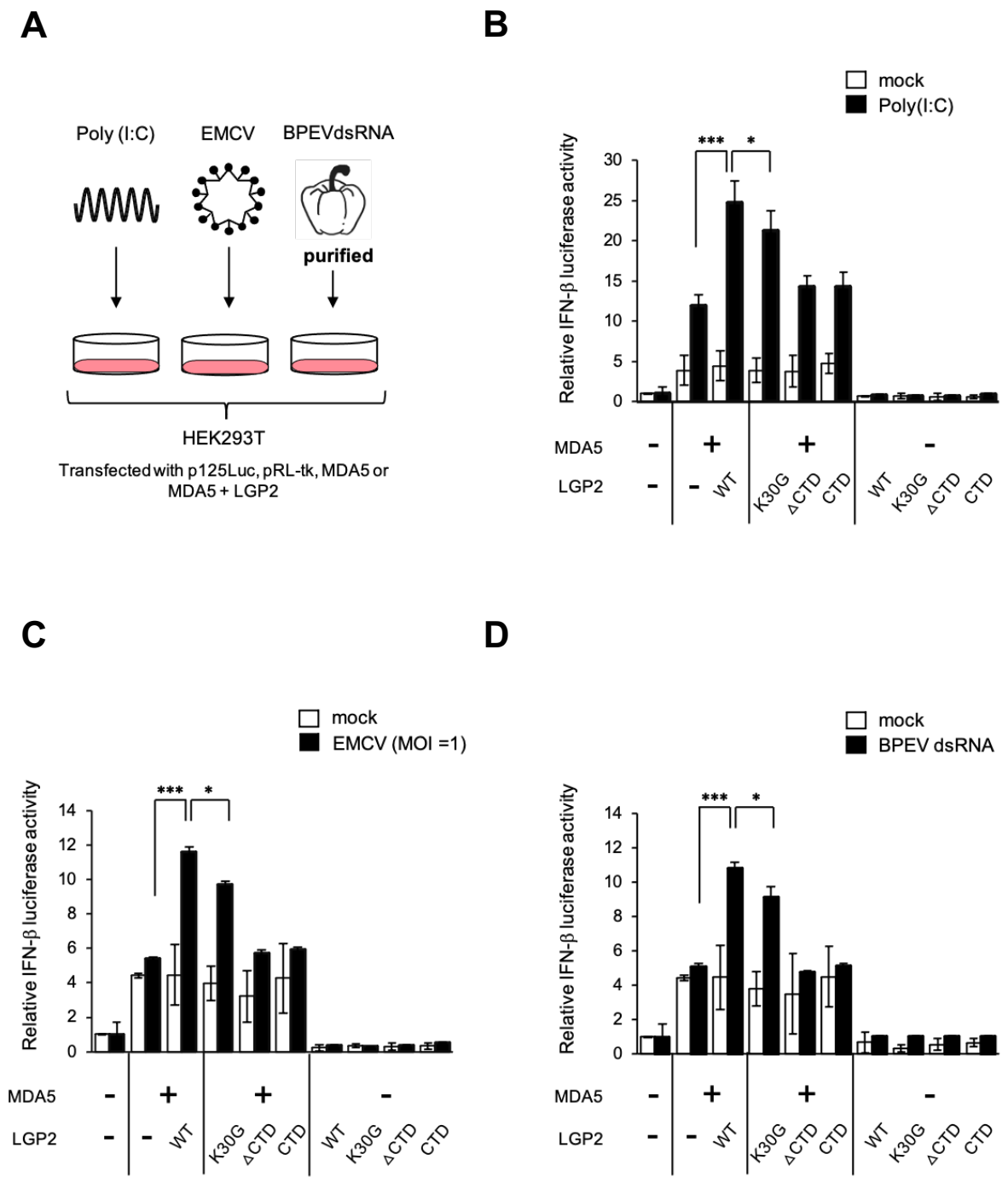

Figure 1. LGP2 and MDA5 co-expression enhance IFN-β promoter activity in response to Poly (I:C), EMCV and BPEVdsRNA. (A) Experimental design to analyze IFN-β promoter activity in HEK293T cells in response to various stimuli. (B-D) HEK293T cells were transfected with a reporter plasmid containing luciferase gene under the control of the IFN-β promoter (p-125Luc), *Renilla* luciferase construct (pRL-tk) as an internal control, 25 ng plasmid expressing MDA5, and 4 ng plasmid expressing LGP2 or its mutant. 24 hours after transfection cells were mock treated, transfected with 3 μg of Poly (I:C) (B), infected with EMCV (MOI = 1) (C), or transfected with 300 ng of BPEVdsRNA (D). After 8 h, cells were subjected to Dual-Luciferase assay. Data shows relative firefly luciferase activity normalized to the *Renilla* luciferase activity, in one of at least three independent experiments, and error bars show ± S.D. *** p <0.001, * p <0.05 unpaired Student's t test.

3.2 LGP2 accelerates MDA5 fiber formation

MDA5 forms fibers by stacking monomers in a head-to-tail manner and strong protein-protein interactions are increasing the affinity for the dsRNA by >100 folds [24, 33, 64]. Mutations in the fiber interfaces result in inability of the protein to form fibers and induce IFN [24], indicating that fiber formation is critical for MDA5 signaling. Previously, it has been reported that LGP2 sensitizes MDA5 to activation by dsRNA [63] and that LGP2 regulates MDA5 fiber assembly [65]. However, the mechanistic basis remained unknown. AFM has been known for visualization of proteins and nucleo-protein complexes [66-68], and here it was utilized to gain an insight into the MDA5 fiber formation in the presence and absence of LGP2 and LGP2 K30G. MDA5 formed fibers slowly, in line with the evidence that MDA5 exhibits slow on rate binding [24]. The fiber formation started after 1-5 minutes of incubation and continued to elongate to reach about 2.5 μm, covering 70% of the BPEVdsRNA after 20 minutes of incubation. In contrast, in the presence of LGP2, fibers formed rapidly, reaching the same length and 70% of BPEVdsRNA occupancy after only 1 minute of incubation (Fig. 2A-B). Interestingly, LGP2 K30G did not enhance MDA5 fiber formation. These results confirmed that LGP2 assisted fiber formation by MDA5, while LGP2 K30G assistance was negligible.

LGP2 alone does not form fibers (top panels Fig. 2A). Therefore, it is necessary to determine whether LGP2 is incorporated into the MDA5-dsRNA fibers. First, height of the fibers formed in the presence or absence of LGP2 was measured. The height of BPEVdsRNA alone was 0.57 nm in average (Fig. 2C-D). MDA5-dsRNA formed 3.6 nm high fibers while in the presence of LGP2 fibers were 4.5 nm high, and 3.9 nm in the presence of LGP2 K30G (Fig. 2C-D). This result indicated LGP2

presence inside the MDA5 fibers. LGP2 K30G participation in the fiber assembly was only a minor.

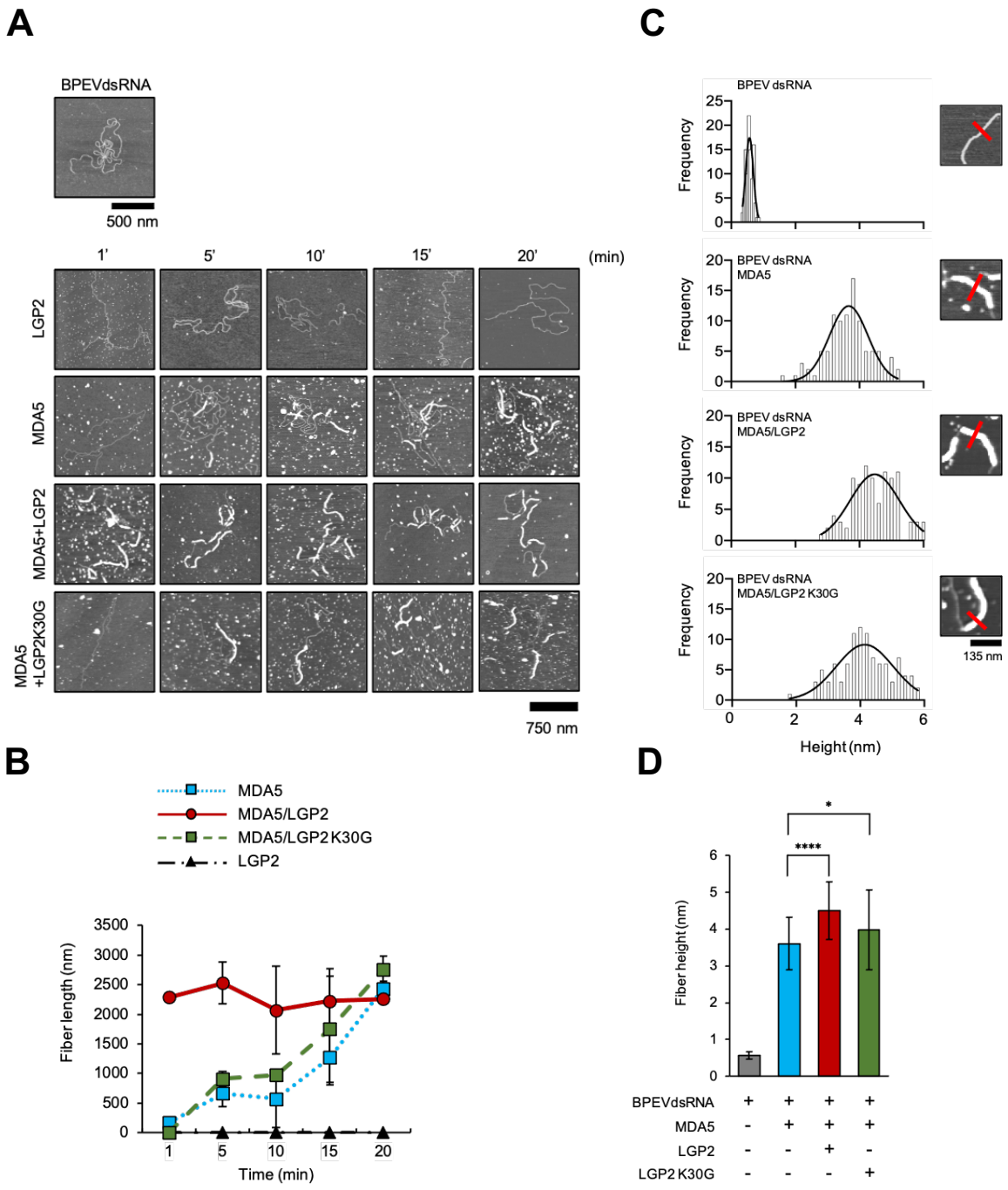

Figure 2. LGP2 accelerates MDA5 fiber formation. (A) AFM images of the MDA5 fiber formation time course in the absence or presence of LGP2 or LGP2 K30G. AFM image of BPEVdsRNA alone (top). (B) The average fiber length measured from at least three independent experiments. Error bars: ± S.D. MDA5 fiber formation. (C) Quantification of the BPEVdsRNA height alone (top) and fibers formed by MDA5, MDA5/LGP2 or MDA5/LGP2 K30G. (D) Average of BPEVdsRNA height (grey), MDA5 fiber height in the absence (blue) and presence of LGP2 (red) or LGP2 K30G (green), measured from 100 sections. Error bars: ± S.D. **** p <0.0001, * p <0.05 unpaired Student's t test.

3.3 LGP2 and MDA5 form hetero-oligomer units

As described above, LGP2 affects the rate of MDA5 fiber assembly, as well as thickness. This data suggested that LGP2 is incorporated into the MDA5/dsRNA fibers. To determine the position of LGP2, specific monoclonal antibody against LGP2 tagged with quantum dot (Qdot655) was used. MDA5 fiber with or without LGP2 was probed with αLGP2-Qdot or control αGFP-Qdot (Fig. 3A). αLGP2-Qdot detected LGP2 within the fiber at various positions, however, did not react with the fiber without LGP2, and significantly lower number of Qdots were observed on MDA5 fibers with LGP2 K30G. Labeled antibody against unrelated protein αGFP-Qdot, did not detect LGP2 in the fiber. Interestingly, LGP2 positioned mostly alternating to the sides of the fibers (Fig. 3C). Number of Qdots per 1 μm of the MDA5 fiber length were counted as shown in the graph (Fig. 3B).

Next, distances between 10 pairs of Qdots were measured. The example of the measurements made is shown (Fig. 3C). The average horizontal distance between two Qdots was 32.8 nm (Fig. 3D). Previous publication showed that 1 molecule of MDA5 occupies 14-15 bp of dsRNA [69]. Taking into account that 15 bp of the stretched dsRNA is ~4.7 nm, it is speculated that one LGP2 molecule exists every 5-9 MDA5 molecules in 32.8 ±8 nm range. These results strongly suggested that MDA5 fibers are indeed composed of LGP2-MDA5 hetero-oligomer units, while LGP2 K30G again failed to demonstrate cooperation in the MDA5 fiber formation.

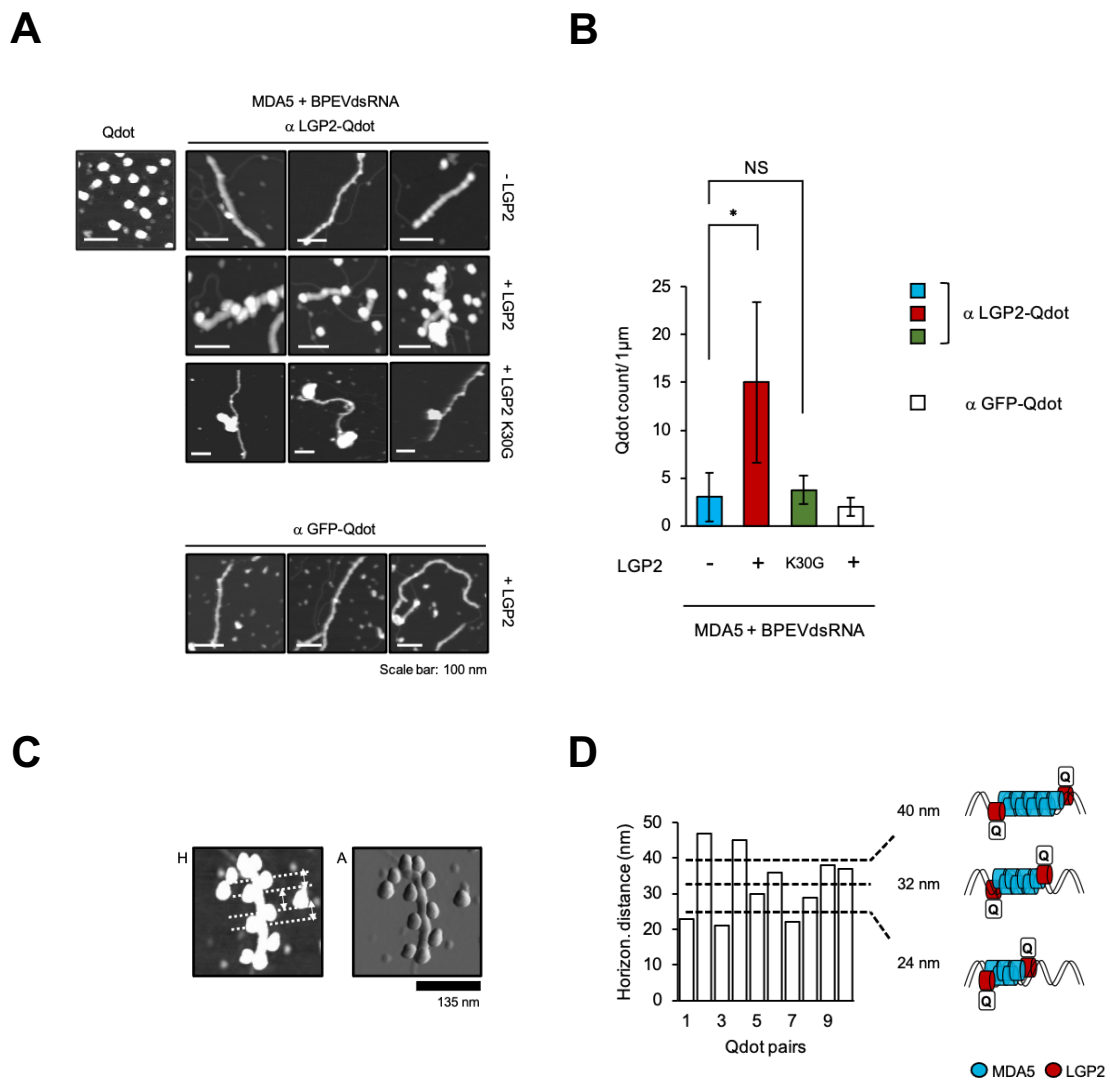

Figure 3. LGP2 is incorporated into the MDA5 fibers. LGP2 antibody against CTD domain was labeled with Qdots, added to the MDA5/LGP2/dsRNA mixture and observed with AFM. (A) AFM images of the MDA5 fibers in the absence (upper panel), presence of LGP2 (middle panel), and LGP2 K30G (lower panel) mixed with αLGP2-Qdot; and in the presence of LGP2 mixed with Qdot labeled antibody against unrelated protein as a control, αGFP-Qdot (bottom panel). (B) Graph shows the average number of Qdots/1 μm of MDA5 fiber length without LGP2 (blue bar), with LGP2 (red bar) and LGP2 K30G (green bar), and MDA5 fibers with LGP2 mixed with αGFP-Qdot (white bar). Error bars: ±S.D. * p <0.05, NS= p >0.05, unpaired Student's t test. (C) Representative AFM image of distance measurements between αLGP2-Qdot attached to the MDA5 fiber. (D) Graph bars show distances between αLGP2-Qdot pairs and the dotted line represents the average distance length between 10 pairs.

3.4 LGP2 promotes MDA5 ATP hydrolysis and fiber turnover

It has been previously described that MDA5 fiber dissociates in the presence of ATP through its hydrolysis [25, 33]. Here, MDA5 fiber dissociation under different conditions was investigated (Fig. 4). First, the role of ATP binding in MDA5 fiber formation was tested. In the presence of ATP, fibers formed faster than in its absence, and upon ATP hydrolysis, MDA5 is released from the end of the fibers, making fiber length shorter after 20 minutes of incubation (~500 nm). In the presence of LGP2, fiber is rapidly disassembled (~500 nm after 1 minute), suggesting higher ATP hydrolysis rate. MDA5 is released mostly from the stem of the BPEVdsRNA (Fig. 4A-B). LGP2 K30G only partially enhanced MDA5 fiber dynamics, suggesting the importance of LGP2 ATPase activity.

To investigate monomeric and oligomeric shifts of MDA5 in the presence of ATP and LGP2, MDA5 fibers were examined by size exclusion chromatography (SEC) (Fig. 4C). The isolated fiber was stable and did not generate free MDA5 spontaneously, as seen by re-chromatography (Fig. 4C panel c). AFM observation revealed that MDA5 fiber dissociates by incubation with ATP, and that is in line with the evidence from the previous research [25]. However, fiber dissociation by incubation with ATP alone was below detectable level by SEC (Fig. 4C panel d). This discrepancy could be due to lower concentration (K_D value) of MDA5 and dsRNA in AFM observation (Materials and Methods). Incubation of the fiber with LGP2 did not generate free MDA5 (Fig. 4C panel e). In contrast, incubation with ATP and LGP2 efficiently dissociated the fiber into free MDA5 (Fig. 4C panel f), suggesting dissociation was dramatically enhanced by LGP2. To investigate the effect of ATP binding and its hydrolysis, AMP-PNP was used, which can bind to ATPase, but it is not hydrolyzed, and LGP2 K30G

as ATP binding deficient mutant. Incubation with AMP-PNP/LGP2 or ATP/LGP2 K30A failed to dissociate the fiber (Fig. 4C panels g and h), suggesting ATP binding and its hydrolysis is involved in the dissociation.

Next, the effect of LGP2 on MDA5 ATPase activity was investigated (Fig. 4D). MDA5 exhibited dsRNA-dependent ATPase activity. Titration of LGP2 to the MDA5/dsRNA mixture, dramatically increased the level of the ATPase activity (Fig. 4D). This observation was the ATP hydrolyzed exclusively by MDA5, because LGP2/dsRNA mixture alone exhibited only the modest level of activity. The enhancing effect of LGP2 was largely lost by K30G mutation. These data indicated highly dynamic events of MDA5 fiber assembly and disassembly in the presence of LGP2 (compare Fig. 2 and Fig. 4). It is clear that ATP facilitates MDA5 binding, while the ATP hydrolysis rate is higher in the presence of LGP2 suggesting fiber turnover and increased number of activated MDA5 molecules.

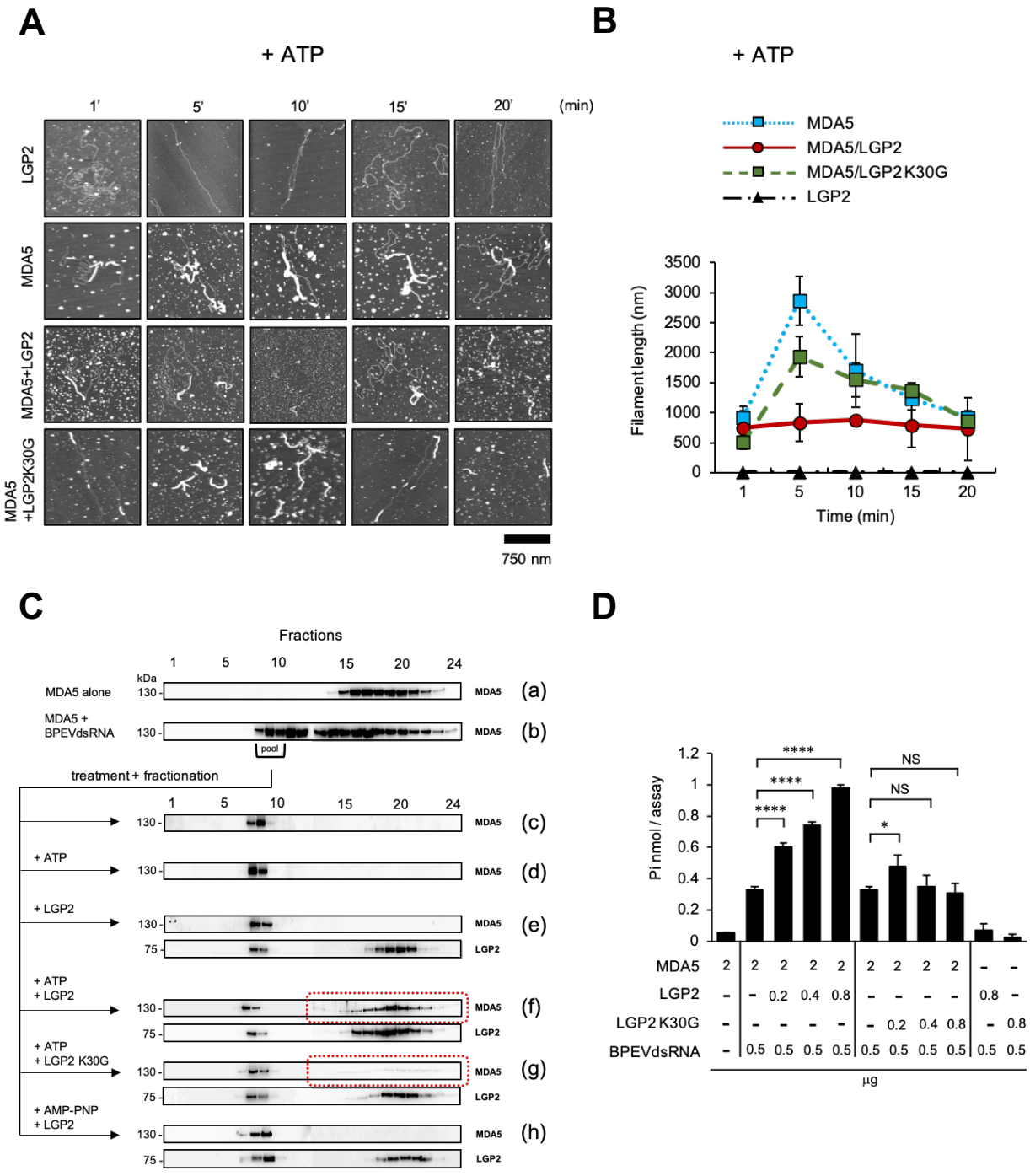

Figure 4. LGP2 promotes MDA5 ATPase activity and fiber dynamics. (A) AFM images of the time course of MDA5 fibers in the presence of ATP and proteins indicated on the left. (B) Average MDA5 fiber length in the presence of ATP and LGP2 or LGP2 K30G. (C) SEC of purified proteins. Fractionation of MDA5 (a) or the reaction mixture of MDA5 and BPEVdsRNA (b) by Sepharose 4B. The high molecular weight fractions (8-10 of b) were pooled as MDA5/BPEVdsRNA fiber. The fiber was re-chromatographed without incubation (c) or after incubation with ATP (d), LGP2 (e), ATP+LGP2 (f), ATP+LGP2 K30G (g), or AMP-PNP+LGP2 (h). Samples were analyzed by immunoblotting (IB) using anti-Flag antibody. (D) ATPase assay. Recombinant proteins were analyzed for ATPase activity (Materials and Methods). Values are average of 3 independent experiments. Error bars: ±S.D. **** p <0.0001, * p <0.05, NS= p >0.05, unpaired Student's t test.

3.5 LGP2 affects MDA5 conformational changes

The exposure of CARDs of MDA5 and RIG-I is the basis for signaling induction and MAVS oligomerization. Protein-RNA complexes were tested for their susceptibility to cleavage by trypsin to further investigate MDA5 CARDs release and activation. 2xFLAG tag placed before N-terminus was used to detect CARDs with anti-Flag antibody and anti-CTD antibody for detection of the C-terminus of MDA5. First, HEK293T cell lysate overexpressing full-length (FL-MDA5) was digested. As shown in Figure 5A, 4 bands arise after trypsin digestion. Band 1 (FL) is uncleaved FL-MDA5 (band 1: ~133 kDa), band 2 (ΔC1) corresponds to the MDA5 with partially cleaved CARD1 (band 2: ~120 kDa) because it was detected by anti-CTD antibody but not by anti-FLAG. Band 3 (ΔCTD) corresponds to the MDA5 lacking C-terminus (band 3: ~115 kDa) because it was detected by anti-FLAG antibody but not by anti-CTD. Band 4 is the MDA5 lacking both, CARD1 and the CTD (ΔC1-CTD) because it could not be detected by either anti-FLAG or anti-CTD. Indeed, N-terminal sequencing revealed that band 4 lacks entire CARD1 (Fig. 5B). It is thus the most important band, corresponding to the protein with open (digested) CARD1 (band 4: ~100 kDa). The same pattern was observed with purified MDA5 after silver staining. Next, it was investigated how ATP and/or LGP2 affect this digestion pattern corresponding to the MDA5 conformational changes. Full length purified proteins are shown (Fig 5C; input). In the absence of a ligand, MDA5 was rapidly digested (Fig. 5C panel a). In the presence of Poly (I:C), MDA5 showed resistance, particularly the helicase domain (Fig. 5C panel c). Nonhydrolyzable ATP binding (AMP-PNP) resulted in MDA5 wrapping around Poly (I:C) more tightly (Fig. 5C panel e). The band intensity from figure 5C, panels e and f were quantified and normalized to the non-digested FL-MDA5 as 100%

(input). In this condition, band 2 was dominant and its intensity increased over time (Fig. 5E). On the contrary, the intensity of band 4 increased gradually as the digestion proceeded. This indicated that CARD1 was partially exposed under these conditions. When LGP2 was present in the fibers (Fig. 5F), band 4 was rapidly detected (after 5 min) and it became dominant as the digestion proceeded. Simultaneously, the band 2 intensity clearly decreased. These results suggested that the presence of LGP2 in the fibers promoted full exposure of CARD1, and possibly CARD2. On the contrary, LGP2 K30G presence showed relatively strong resistance of the band 3 in all conditions, which corresponds to closed CARDs (Fig. 5D, G). Interestingly, band 4 resistance was also observed, although appearing slower. Taken all together, presence of LGP2 K30G resulted in a mixture of active and non-active MDA5 molecules, possibly due to inability of this mutant to bind ATP and change the conformation.

Interestingly, when ATP was added instead of AMP-PNP (Fig. 5C panels g and h), the digestion pattern was almost identical to that of AMP-PNP (Fig. 5C panels e and f). Figure 4C, panel f showed that MDA5/LGP2/dsRNA complex with ATP, but not AMP-PNP, resulted in dissociation. Since naïve MDA5 is highly sensitive to trypsin digestion (Fig. 5C, a), this result suggested that MDA5 was released from the fibers through ATP hydrolysis. Furthermore, even after the dissociation, MDA5 retained a structure similar to that bound to the dsRNA. To test this hypothesis, the MDA5/Poly(I:C) complex was isolated by SEC. The fiber was mixed with ATP and LGP2 to accelerate dissociation. Ultracentrifugation was used to separate fiber (pellet) from dissociated protein (supernatant). Native-PAGE (Fig. 5H) revealed that the released MDA5 is composed of monomers and oligomers. Trypsin digestion of this released MDA5 (supernatant) exposed CARD1 (Fig. 5I) as compared to the naïve MDA5 which CARD1 remained trypsin resistant.

This data indicated that MDA5 changes conformation in the presence of a ligand and during ATP binding and hydrolysis. LGP2 clearly appears as a catalyst in this reaction, keeping MDA5 highly flexible. While MDA5 is still able to signal by itself, this data suggested that signaling is limited and LGP2 is able to facilitate CARDs release for the signaling.

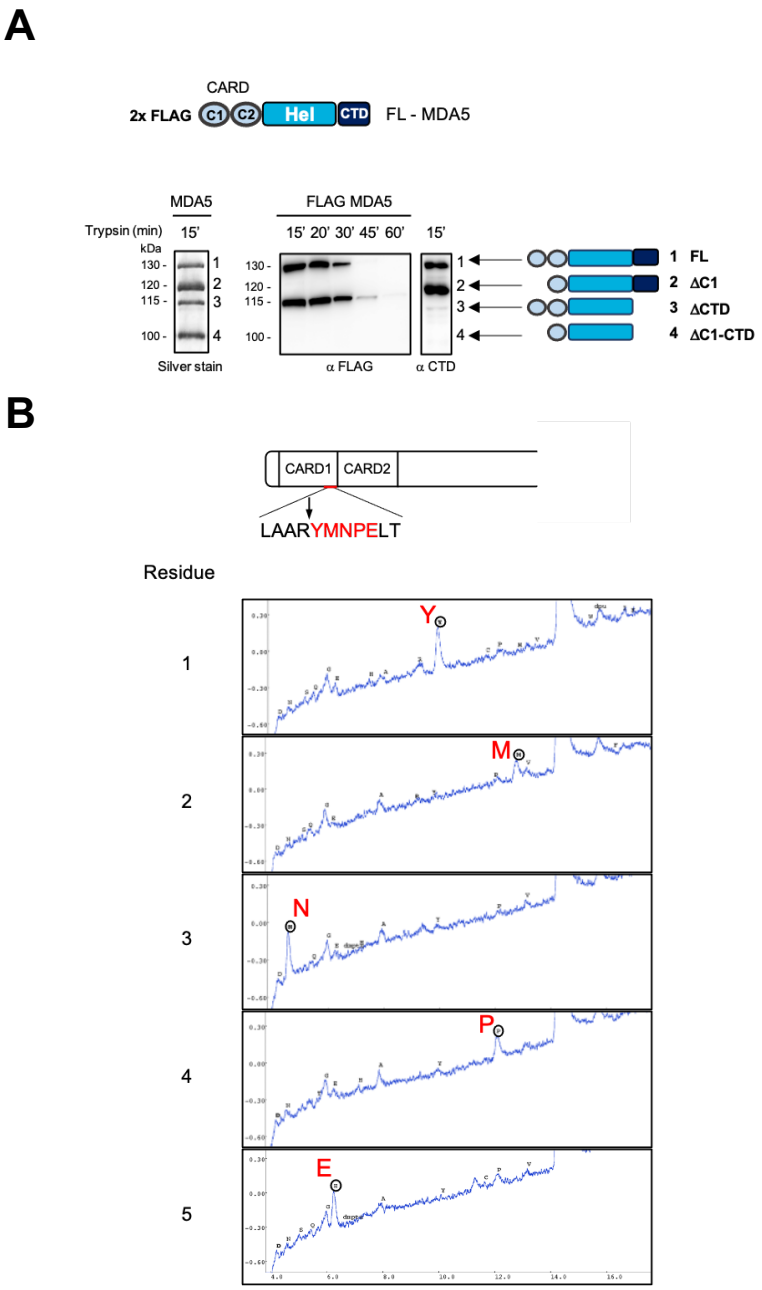

Figure 5. LGP2 shows the ability to affect MDA5 CARDs exposure. (A) MDA5 trypsin digestion pattern. Anti-Flag antibody was used to detect N-terminal of MDA5 and anti-MDA5-CTD was used to detect C-terminal of the protein. In the schematic representation, the accessible cleavage sites are shown resulting in the observed 4 bands, indicated by 1,2,3 and 4 arrows. (B) N-terminal sequencing of band 4 produced by limited trypsin digestion of MDA5.

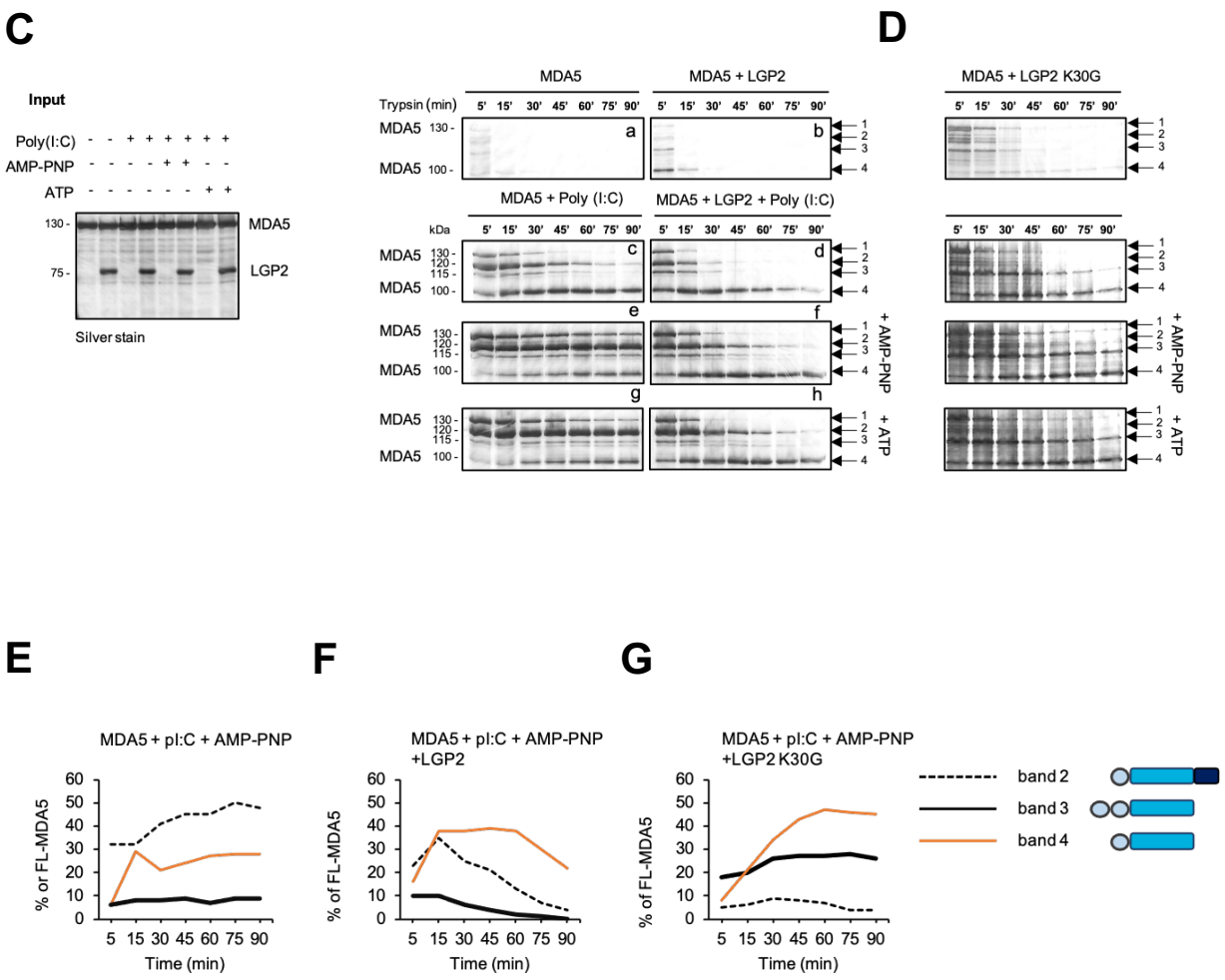

Figure 5. LGP2 shows the ability to affect MDA5 CARDs exposure. (C) Silver stained time course of trypsin treated (35 ng) purified MDA5 in the absence (upper panel) and presence (lower panels) of Poly (I:C); left and right panels show MDA5 tryptic digestion in the absence and presence of LGP2 respectively with addition of AMP-PNP and ATP where indicated, and (D) in the presence of LGP2 K30G. (E-G) Graphs show intensity of band 2, 3 and 4 that indicated opening of the CARDs over an indicated time in the presence of Poly (I:C) and AMP-PNP, LGP2 or LGP2 K30G; values are expressed as percentage if non-digested FL-MDA5 represents 100% (input).

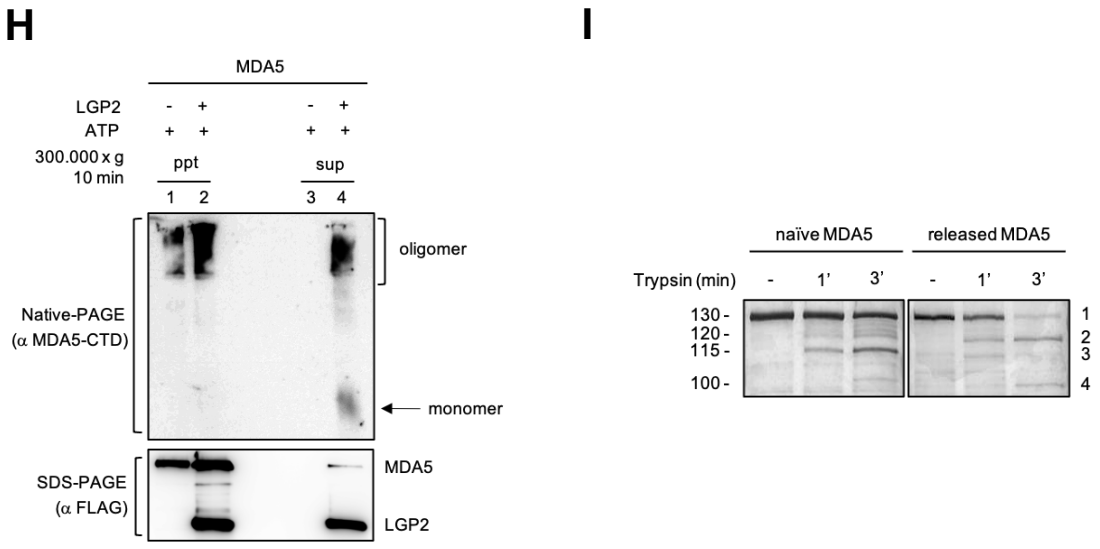

Figure 5. LGP2 shows the ability to affect MDA5 CARDs exposure. (H) Native-PAGE analysis of MDA5/Poly (I:C) complex. MDA5/Poly (I:C) complex was isolated by SEC as in Fig. 4Ab, followed by the complex incubation with ATP in the presence or absence of LGP2. The mixture was ultracentrifuged into Poly (I:C)-bound complex (ppt) and released proteins (sup). The fractions were analyzed by native (top) and SDS (bottom) PAGE and subjected to immunoblotting with anti-MDA5 antibody (top) and-Flag antibody (bottom). (I) Trypsin digestion of MDA5. Naïve recombinant MDA5 and dissociated MDA5 (from lane 4 in Fig. 5H) were analyzed by limited trypsin digestion as in (C). Positions of full length MDA5 (1) and its digestion products (2-4) are shown on the right.

3.6 MDA5 autoinhibition in the absence of infection

As mentioned above, inactive MDA5 is rapidly digested and tryptic resistance appears with the presence of a ligand. In the case of RIG-I, CARDs are locked in the ligand-free environment, and only the presence of the RNA is inducing the conformational change in the CTD and subsequent liberation of the CARDs [18-20]. Interestingly, RIG-I shows equal resistance with and without a ligand but different conformation [70]. To detected which band appears first in the absence of a ligand, amount of trypsin and time of the treatment were reduced. First digested part of MDA5 was CTD, while CARDs were still protected. This indicated that inactive MDA5 takes conformation where CTD is free to scan the cytoplasm for a foreign RNAs, while CARDs are not exposed (Fig. 6A). If the CARDs are being held locked, auto-inhibition mechanism must be different to that of RIG-I. This data indicated that MDA5, as well as RIG-I, possesses auto-inhibited conformation, however, this state is rather weak and presumably easily disrupted.

A single amino acid substitution in MDA5 (G821S) results in the constitutive production of IFN-I and inflammatory cytokines, and autoimmunity-like phenotype in mice [55]. Here, MDA5 wild type and G821S single molecule were observed by AFM. This revealed that MDA5 wild type adopts an open structure, composed of 3 to 4 subdomains and connecting linkers (Fig. 6B, left). However, G821S exhibited a closed, globular structure (Fig. 6B, right). Furthermore, this was confirmed by a high-speed AFM observation of a single molecule (Fig. 6C). Examination of these molecules by limited trypsin digestion revealed that the conformation of MDA5 and G821S were distinct. CARDs were mostly masked in MDA5 wild type but highly sensitive (exposed) in G821S (Fig. 6A, right). In summary, wild type MDA5 has an open structure but the

CARDs are masked, whereas the overall structure of G821S is closed with a sensitive, fully exposed CARDs. These results prompted the comparison of the molecular structure of MDA5 after its interaction with dsRNA and ATP or LGP2, by AFM (Fig. 6D, E, F). As a result, MDA5 interacted with dsRNA, dissociated and then underwent major structural change from an open to a closed conformation, in which the CARD1 was unmasked.

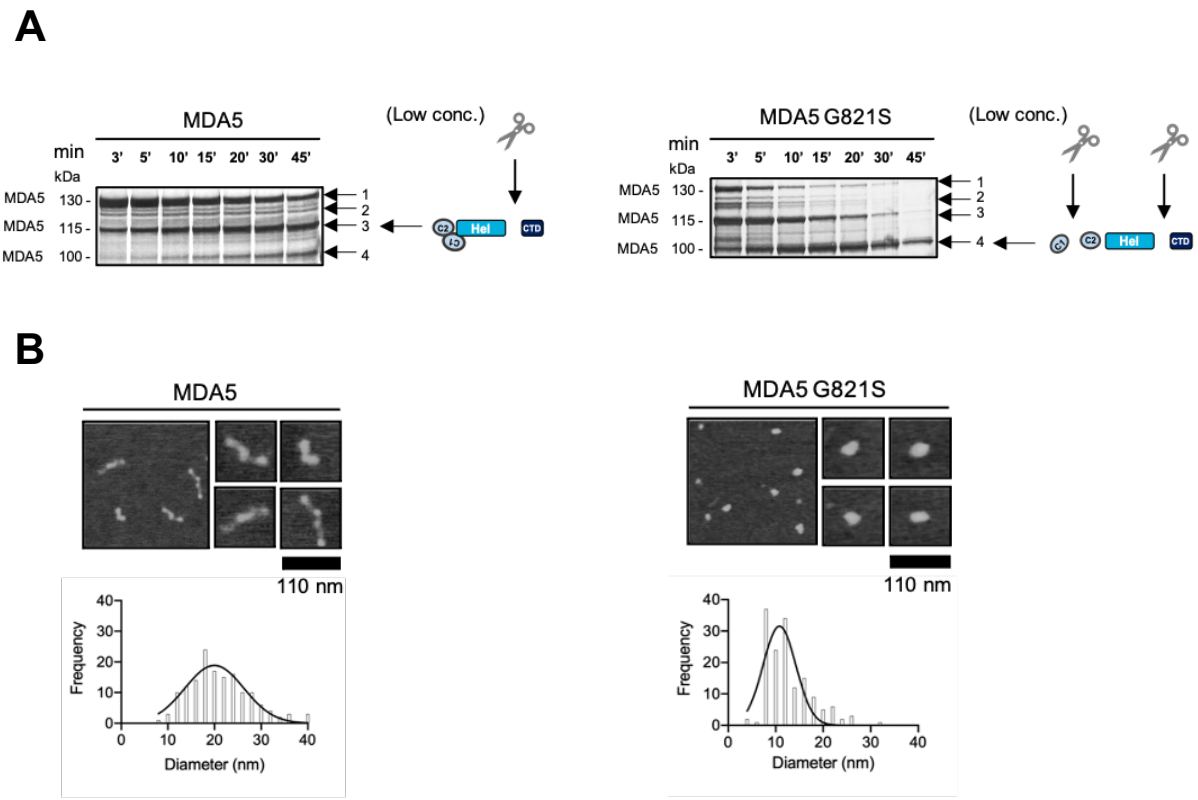

Figure 6. Trypsin digestion and AFM observation of recombinant MDA5 wt and MDA5 G821S
(A) Recombinant MDA5 and MDA5 G821S were digested with trypsin as described in Figure 5C a, except with a lower trypsin concentration (TPCK trypsin 17 ng) and shorter incubation time. (B) AFM analyses of MDA5 and MDA5 G821S. AFM images of MDA5 and MDA5 G821S. Left: 300 x 300-nm^2 images, Right: 75 x 75-nm^2 images. From these images, MDA5 monomers (objects with a total volume of 300±30 nm^3) were selected and quantified for diameter (bottom).

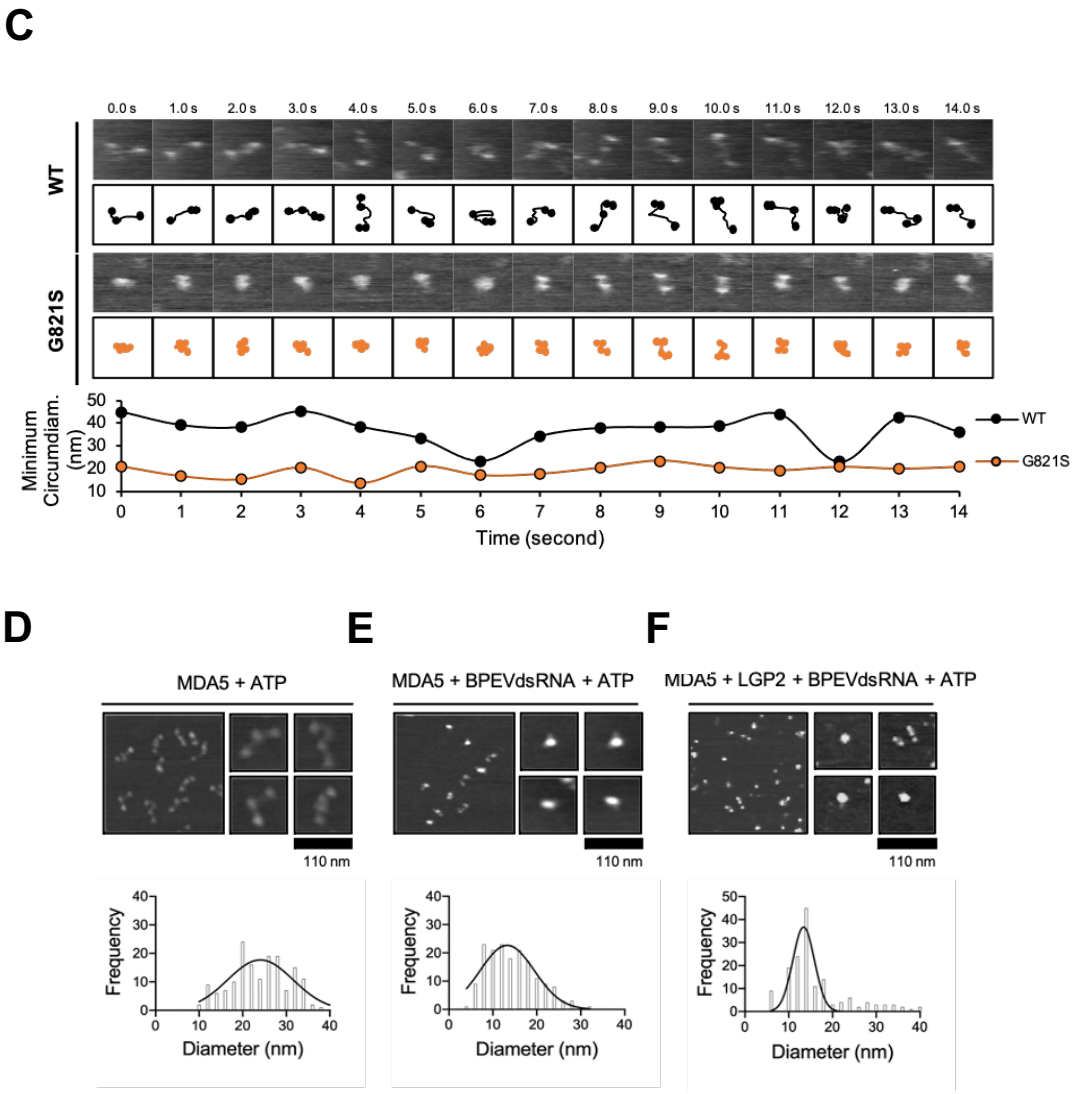

Figure 6. Trypsin digestion and AFM observation of recombinant MDA5 wt and MDA5 G821S
(C) Single-molecule analysis of WT and G821S using high-speed AFM. Images are 62.5 x 62.5-nm^2 frames acquired at a rate of 1 frame per second. Schematic representation of each image is displayed below. Representative live images are shown. The minimum circum-diameter (MCD) of each frame is shown (bottom). (D) AFM images of MDA5 protein under different conditions. Wild type MDA5 was incubated with reaction buffer (D) or with dsRNA (E) or with dsRNA and LGP2 (F), in the presence of 1 mM ATP for 30 min. Left: 300 x 300 nm2 images, Right: 75 x 75-nm2 images. From these images, MDA5 monomers (objects with total volume of 300±30 nm^3) were selected and quantified for diameter (bottom).

3.7 Proposed model for MDA5/LGP2 signaling

Based on the data presented above, a mechanistic model by which LGP2 augments MDA5 signaling is proposed. In line with the previous evidence, LGP2-mediated RNA recognition enabled MDA5 to nucleate fiber assembly at more locations along dsRNA at the same time. Physiologically, the presence of ATP is of great importance. Here, the mechanism of MDA5 fiber formation in the presence or absence of LGP2 and ATP is illustrated (Illustration 5).

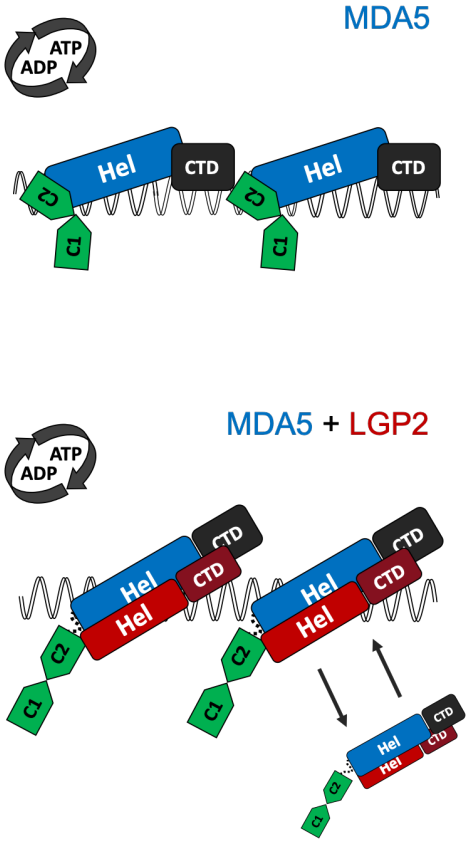

Illustration 5: MDA5 conformation in the absence (top) and presence (bottom) of LGP2 and ATP

From the AFM data, it can be concluded that fibers are assembled and disassembled rapidly in the presence of ATP and LGP2. This suggests highly dynamic events with more fiber turnover opportunities, resulting in dramatically increased number of signaling competent MDA5 molecules. It was previously reported that MDA5 fibers are dissociated through ATP hydrolysis [25, 33]. The ATP-dependent dissociation is sometimes interpreted as a negative mechanism of signaling regulation, preventing the self-RNA recognition. However, the addition of LGP2 and ATP to pre-formed MDA5 fibers promoted efficient fiber dissociation (Fig. 4C), suggesting that the dissociation is related to the positive regulation of signaling.

The exposure and oligomerization of the tandem CARD is a trigger of antiviral signaling by RLR (C1 and C2, Fig. 5A) through conformational change [1, 24, 25, 71, 72].

To investigate structural changes and CARDs release, MDA5/Poly (I:C) complexes were tested for their susceptibility to cleavage by trypsin. The naïve MDA5 molecule has an open structure and exhibited hypersensitivity to trypsin digestion. This is consistent with the AFM observation of a single MDA5 molecule [55]. MDA5 binding to the RNA induced a structural change where CARDs are exposed (Fig. 5C). ATP binding caused further changes, as demonstrated in the presence of AMP-PNP, MDA5 binds RNA more tightly and CARD1 is only partially exposed. These fibers are long, non-flexible and with only few locations from where protein could be released for a turnover. Addition of LGP2 promoted full exposure of the CARD1 and the CTD. It is very likely that the CARD2 is exposed as well, oligomerized and more resistant to the tryptic digestion. It appears that enzymatically inactive LGP2 K30G was not fully able to demonstrate augmentation of MDA5/dsRNA binding or CARDs exposure. If this is the consequence of mutant LGP2 having different conformation or lower RNA affinity, remains to be elucidated. Surprisingly, in the presence of ATP, which promotes fiber dissociation, the MDA5 conformation is identical to that within the fibers. This indicated that the dissociated free MDA5 did not adopt the conformation of an inactive protein. It retained its “activated” conformation with the exposed CARD1. This could mean that the MDA5 has a “memory” of encountering a viral RNA even after the release and this model is consistent with the AFM observation of the MDA5 structure (Fig. 6D).

The conformational changes of MDA5 through interaction with dsRNA, LGP2 and ATP is shown step-by-step in Figure 7. The activated MDA5 may migrate to downstream adaptor MAVS to form aggregates and trigger the signaling cascade, leading to the activation of IFN and IFN-stimulated genes.

In summary, it was strongly suggested that ATP is essential for MDA5 fiber formation and production of free MDA5 in the activated conformation through its

hydrolysis, where LGP2 is a reaction catalyst in each step, thus being the key positive regulator of the viral RNA recognition.

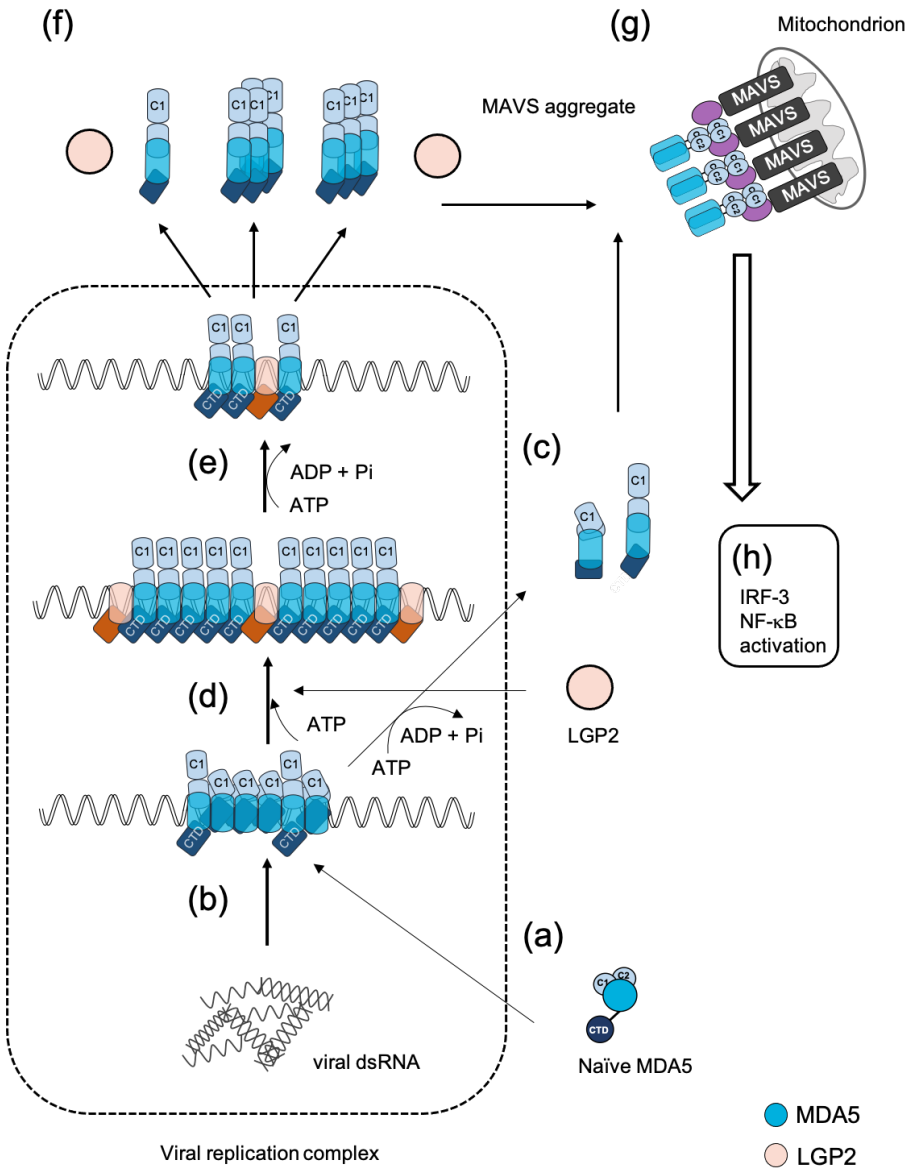

Figure 7. MDA5 activation by LGP2 and ATP (a) Inactive MDA5 has an open conformation, keeping the tandem CARD masked. (b) Upon binding with viral dsRNA within the viral replication complex, MDA5 forms fibers. The conformation is closed with only partially exposed CARD1. (c) ATP hydrolysis weakly promotes MDA5 release from the dsRNA. (d) In the presence of LGP2 and ATP, MDA5 conformation is further changed to fully exposed CARD1. (e) Upon ATP hydrolysis, the fiber efficiently dissociates. (f) Released MDA5 retains its open conformation as monomer/oligomer mixture, it exits from the viral replication complex and migrates to its downstream adaptor, MAVS. (g) MDA5 CARDs form a complex with the CARD of MAVS on mitochondria. (h) Aggregation of MDA5 and MAVS results in the activation of transcription factors, including IRF-3 and NF-κB.

Chapter 4

Discussion

DISCUSSION

MDA5 is an RNA sensor that has ability to recognize viral infections and initiate an antiviral response. MDA5 is implicated in a range of autoimmune disorders. Therefore, investigation of the MDA5 activation mechanism is of great importance. MDA5 is activated upon recognition and binding of long dsRNA and ATP. The exposure of CARDs enables interaction with a downstream partner MAVS. However, considering low RNA binding affinity, activation of MDA5 may require more than just RNA binding. The binding is initial step towards IFN induction and fiber formation is shown to be requirement [69], but this is an initiation of the cascade of the events leading to an activated MDA5. RLRs are expressed at low levels inside the cells. While inactive RIG-I is able to take auto-repressed form, it was unknown what conformation endogenous inactive MDA5 takes, what is the role of ATP hydrolysis and what are the mechanisms by which other accessory proteins, such as LGP2, can regulate MDA5 activation. The data presented here demonstrate that LGP2 is a requisite partner in the mechanism of MDA5 activation.

LGP2 has the ability to enhance IFN-β through MDA5 in response to three different types of stimulation: synthetic RNA mimic (Poly (I:C)), virus (EMCV) and natural viral dsRNA (BPEVdsRNA). Full length LGP2 necessity, as well as fully functional ATP binding site, demonstrated the importance of its helicase domain and that augmentation of MDA5 signaling is not only result of stronger LGP2 affinity for the dsRNA. Moreover, the amino acid region in domain IV is completely conserved between MDA5 and LGP2. Deletion of this region, completely abolished ability of LGP2 to augment MDA5 signaling [63]. This region has also been shown to be critical in response to paramyxovirus V proteins which are able to disrupt MDA5-LGP2

association [10, 11]. Taken all together, it is tempting to think that MDA5/LGP2 interaction through their helicases is a critical step in displacing the MDA5 CARDs for the signaling.

MDA5 fiber formation is rapid in the presence of LGP2. MDA5 alone shows faster fiber formation only in the presence of ATP. AFM data and ATPase assay demonstrated that in the presence of both, LGP2 and ATP, fibers are assembled and disassembled even more rapidly. Thus, LGP2 presence inside the fiber is not only keeping the CARDs displaced for signaling, but also creating the opportunity for ATP hydrolysis and dissociation from the RNA at several locations. Possibility of fiber turnover and more activated MDA5 molecules are certain. Furthermore, this reveals possible answer to the current question in the filed: why MDA5 fibers were never captured in the living cells. This study has shown that these events are highly dynamic.

Crystal structures have revealed the details of MDA5 bound to RNA. However, what has not been shown by crystallography so far, is the position and movement of CARDs, presumably due to their flexibility. Here, trypsin digestion was utilized to reveal conformational changes of the FL-MDA5. Naïve MDA5 is incompetent for signaling. For example, cellular treatment of IFN-I induces MDA5 expression, but does not activate IRF-3 or NF-κB nor subsequent IFN-I genes. This means that naïve MDA5 is in inactive conformation, and CARDs are not available. The mechanism by which the MDA5 CARDs are sequestered in the inactive state is so far unknown. This could be different from RIG-I. In RIG-I, Hel2i region interacts with CARDs keeping the protein inactive in the absence of infection. In MDA5 Hel2i region is shorter. Furthermore, there is no interaction between CARDs and CARD-deleted MDA5 [25]. These differences suggest distinct mechanism of sequestration between MDA5 and RIG-I. However, Figure 6A shows that inactive MDA5 does not expose CARDs: Band 3 (as

a hallmark of closed CARDs) appears first, and it is resistant to trypsin. This suggested that sequestration mechanism exists. Linker region between the CARDs and a helicase emerged as a candidate for future investigation in a role of keeping the CARDs unavailable in the absence of infection.

Presence of a ligand showed resistant MDA5, indicating conformational change from the inactive MDA5 molecule. These fibers have exposed CARDs and trypsin sensitive CTD. Adding AMP-PNP to the solution, results in MDA5 retracting the CARD and it shows resistant CTD. In contrast, in the presence of LGP2, addition of AMP-PNP did not cause retraction of the CARDs and MDA5 was able to fully expose CARD1 and trypsin sensitive CTD. This can be explained by differential twisting of the helicase in these two conditions (MDA5 alone vs MDA5/LGP2), where the later still retains higher flexibility and needs lower energy to dissociate from the RNA upon ATP hydrolysis, as well as ability to nucleate a new set of MDA5 molecules (exposed CTD). This is in line with the major difference in the orientation of the CTD between RIG-I and MDA5. The long axis of the CTD is parallel to the dsRNA and leaves ~30° gap between Hel1 and the CTD of the MDA5 [24]. This gives MDA5 a C-shaped ring structure around the dsRNA, while RIG-I is known to form O-shaped ring with CTD ~20° tilted towards the dsRNA. ATP binding can stabilize, and hydrolysis can destabilize fibers. LGP2 is accelerating binding and lowering the energy required for the reaction while creating multiple short fibers, more opportunities for hydrolysis and new nucleation sites: it is tempting to hypothesize that LGP2 is governing the reaction start and reaction end.

The details of the negative role of LGP2 in innate immune signaling, remain to be elucidated. There are several hypotheses how LGP2 exerts its negative role, particularly in case of RIG-I signaling. One is that LGP2 reduces IRF3 activation, for

example in NDV and SV infected cells [26]. Another one is that LGP2 inhibits TRAF ubiquitin ligase [73] and interacts with MAVS [12]. Possibly, low amounts of LGP2 are able to positively regulate MDA5 because of its ability to sensitize MDA5 to MAVS more rapidly, considering our data that CARDs are exposed. High amounts of LGP2 interacting with MAVS will block MDA5 from associating with MAVS. This also can contribute to our hypothesis of LGP2 being a regulating switch, a fine line between positive and negative role is in its concentration levels inside the cells. Moreover, one group reported that LGP2 expression is enhanced by IRF3 in Olive Flounder [74]. It would be of interest to investigate if rising levels of IRF3 (in human) are inducing expression of LGP2, bringing it to a level of a negative role to stop the IFN induction. This simply could represent a negative feedback loop, a crucial step in preventing autoimmunity.

Hypersensitive MDA5 and defects in factors that repress MDA5 function have been identified as features of several autoimmune disorders, as described in section 1.4. A fine balance between activation and countering the activity to prevent inflammation must be tightly regulated. ATP turnover is a critical part of sensing and signaling by RLRs. Moreover, RLRs defective for ATP binding or hydrolysis are gain-of-function or loss-of-function mutants, which puts ATPase activity in the spotlight as one of the most important features in keeping the balance of activation and repression in order. LGP2 appears to be a catalyst in this reaction for MDA5. The ability of LGP2 to augment MDA5 dsRNA binding, ATP hydrolysis, fiber turnover and conformational changes is without a doubt critical in this balancing mechanism. Therefore, future investigation of LGP2 in the context of autoimmune disorders could give us some insights into the possible causes as well as therapy targets.

In conclusion, although there is still much work to be done, it is clear that LGP2 could be our guide to a better understanding of the mechanisms regulating MDA5 innate immune signaling. Since both, MDA5 and LGP2, are implicated in the roles beyond antiviral signaling, their synergism calls for urge to be investigated in depth.

Chapter 5

Bibliography

BIBLIOGRAPHY

1. Yoneyama,M., Kikuchi,M., Natsukawa,T., Shinobu,N., Imaizumi,T., Miyagishi,M., Taira,K., Akira,S. and Fujita,T. (2004) The RNA helicase RIG-I has an essential function in double-stranded RNA-induced innate antiviral responses. *Nat. Immunol.*, **5**, 730–737.
2. Kawai,T. and Akira,S. (2009) The roles of TLRs, RLRs and NLRs in pathogen recognition. *Int. Immunol.*, **21**, 317–337.
3. Onomoto,K., Onoguchi,K., Takahasi,K. and Fujita,T. (2010) Type I interferon production induced by RIG-I-like receptors. *J. Interf. Cytokine Res.*, **30**, 875–881.
4. Kato,H., Takeuchi,O., Sato,S., Yoneyama,M., Yamamoto,M., Matsui,K., Uematsu,S., Jung,A., Kawai,T., Ishii,K.J., *et al.* (2006) Differential roles of MDA5 and RIG-I helicases in the recognition of RNA viruses. *Nature*, **441**, 101–105.
5. Wies,E., Wang,M.K., Maharaj,N.P., Chen,K., Zhou,S., Finberg,R.W. and Gack,M.U. (2013) Dephosphorylation of the RNA Sensors RIG-I and MDA5 by the Phosphatase PP1 Is Essential for Innate Immune Signaling. *Immunity*, **38**, 437–449.
6. Kumar,H., Kawai,T., Kato,H., Sato,S., Takahashi,K., Coban,C., Yamamoto,M., Uematsu,S., Ishii,K.J., Takeuchi,O., *et al.* (2006) Essential role of IPS-1 in innate immune responses against RNA viruses. *J. Exp. Med.*, **203**, 1795–1803.
7. Liu,S., Chen,J., Cai,X., Wu,J., Chen,X., Wu,Y.-T., Sun,L. and Chen,Z.J. (2013) MAVS recruits multiple ubiquitin E3 ligases to activate antiviral signaling cascades. *Elife*, **2**, 1–24.
8. Ramos,H.J. and Gale,M. (2011) RIG-I like receptors and their signaling crosstalk in the regulation of antiviral immunity. *Curr. Opin. Virol.*, **1**, 167–176.
9. Myong,S., Cui,S., Cornish,P. V, Kirchhofer,A., Gack,M.U., Jung,J.U., Hopfner,K.-P. and Ha,T. (2009) Cytosolic Viral Sensor RIG-I Is a 5'-Triphosphate–Dependent Translocase on Double-Stranded RNA. *Science (80-.).*, **323**, 1070 LP – 1074.

10. Deddouche,S., Goubau,D., Rehwinkel,J., Chakravarty,P., Begum,S., Maillard,P. V., Borg,A., Matthews,N., Feng,Q., van Kuppeveld,F.J.M., *et al.* (2014) Identification of an LGP2-associated MDA5 agonist in picornavirus-infected cells. *Elife*, **2014**, 1–20.
11. Parisien,J.-P., Bamming,D., Komuro,A., Ramachandran,A., Rodriguez,J.J., Barber,G., Wojahn,R.D. and Horvath,C.M. (2009) A Shared Interface Mediates Paramyxovirus Interference with Antiviral RNA Helicases MDA5 and LGP2. *J. Virol.*, **83**, 7252–7260.
12. Komuro,A. and Horvath,C.M. (2006) RNA- and Virus-Independent Inhibition of Antiviral Signaling by RNA Helicase LGP2. *J. Virol.*, **80**, 12332–12342.
13. Yoneyama,M., Kikuchi,M., Matsumoto,K., Imaizumi,T., Miyagishi,M., Taira,K., Foy,E., Loo,Y.-M., Gale,M., Akira,S., *et al.* (2005) Shared and Unique Functions of the DExD/H-Box Helicases RIG-I, MDA5, and LGP2 in Antiviral Innate Immunity. *J. Immunol.*, **175**, 2851–2858.
14. Bamming,D. and Horvath,C.M. (2009) Regulation of signal transduction by enzymatically inactive antiviral RNA helicase proteins MDA5, RIG-I, and LGP2. *J. Biol. Chem.*, **284**, 9700–9712.
15. Satoh,T., Kato,H., Kumagai,Y., Yoneyama,M., Sato,S., Matsushita,K., Tsujimura,T., Fujita,T., Akira,S. and Takeuchi,O. (2010) LGP2 is a positive regulator of RIG-I- and MDA5-mediated antiviral responses. *Proc. Natl. Acad. Sci. U. S. A.*, **107**, 1512–1517.
16. Bruns,A.M., Pollpeter,D., Hadizadeh,N., Myong,S., Marko,J.F. and Horvath,C.M. (2013) ATP hydrolysis enhances RNA recognition and antiviral signal transduction by the innate immune sensor, laboratory of genetics and physiology 2 (LGP2). *J. Biol. Chem.*, **288**, 938–946.
17. Pippig,D.A., Hellmuth,J.C., Cui,S., Kirchhofer,A., Lammens,K., Lammens,A., Schmidt,A., Rothenfusser,S. and Hopfner,K.-P. (2009) The regulatory domain of the RIG-I family ATPase LGP2 senses double-stranded RNA. *Nucleic Acids Res.*, **37**, 2014—2025.
18. Ramanathan,A., Devarkar,S.C., Jiang,F., Miller,M.T., Khan,A.G., Marcotrigiano,J. and Patel,S.S. (2016) The autoinhibitory CARD2-Hel2i Interface of RIG-I governs RNA selection. *Nucleic Acids Res.*, **44**, 896–909.
19. Luo,D., Ding,S.C., Vela,A., Kohlway,A., Lindenbach,B.D. and Pyle,A.M. (2011) Structural insights into RNA recognition by RIG-I. *Cell*, **147**, 409–422.

20. Kowalinski,E., Lunardi,T., McCarthy,A.A., Louber,J., Brunel,J., Grigorov,B., Gerlier,D. and Cusack,S. (2011) Structural basis for the activation of innate immune pattern-recognition receptor RIG-I by viral RNA. *Cell*, **147**, 423–435.
21. Zhang,M., Wu,X., Lee,A.J., Jin,W., Chang,M., Wright,A., Imaizumi,T. and Sun,S.C. (2008) Regulation of IκB kinase-related kinases and antiviral responses by tumor suppressor CYLD. *J. Biol. Chem.*, **283**, 18621–18626.
22. Bruns,A.M. and Horvath,C.M. (2012) Activation of RIG-I-like receptor signal transduction. *Crit. Rev. Biochem. Mol. Biol.*, **47**, 194–206.
23. Peisley,A., Wu,B., Yao,H., Walz,T. and Hur,S. (2013) RIG-I Forms Signaling-Competent Filaments in an ATP-Dependent, Ubiquitin-Independent Manner. *Mol. Cell*, **51**, 573–583.
24. Wu,B., Peisley,A., Richards,C., Yao,H., Zeng,X., Lin,C., Chu,F., Walz,T. and Hur,S. (2013) Structural basis for dsRNA recognition, filament formation, and antiviral signal activation by MDA5. *Cell*, **152**, 276–289.
25. Berke,I.C. and Modis,Y. (2012) MDA5 cooperatively forms dimers and ATP-sensitive filaments upon binding double-stranded RNA. *EMBO J.*, **31**, 1714–1726.
26. Rothenfusser,S., Goutagny,N., DiPerna,G., Gong,M., Monks,B.G., Schoenemeyer,A., Yamamoto,M., Akira,S. and Fitzgerald,K.A. (2005) The RNA Helicase Lgp2 Inhibits TLR-Independent Sensing of Viral Replication by Retinoic Acid-Inducible Gene-I. *J. Immunol.*, **175**, 5260–5268.
27. Myong,S., Cui,S., Cornish,P. V, Kirchhofer,A., Gack,M.U., Jung,J.U., Hopfner,K.-P. and Ha,T. (2009) Cytosolic Viral Sensor RIG-I Is a 5'-Triphosphate–Dependent Translocase on Double-Stranded RNA. *Science (80-.).*, **323**, 1070 LP – 1074.
28. Anchisi,S., Guerra,J. and Garcin,D. (2015) RIG-I atpase activity and discrimination of self-RNA versus non-self-RNA. *MBio*, **6**, 1–12.
29. Louber,J., Brunel,J., Uchikawa,E., Cusack,S. and Gerlier,D. (2015) Kinetic discrimination of self/non-self RNA by the ATPase activity of RIG-I and MDA5. *BMC Biol.*, **13**, 11–14.
30. Rawling,D.C., Fitzgerald,M.E. and Pyle,A.M. (2015) Establishing the role of ATP for the function of the RIG-I innate immune sensor. *Elife*, **4**, 1–21.

31. Lässig,C., Matheisl,S., Sparrer,K.M.J., Mann,C.C. d. O., Moldt,M., Patel,J.R., Goldeck,M., Hartmann,G., García-Sastre,A., Hornung,V., *et al.* (2015) ATP hydrolysis by the viral RNA sensor RIG-I prevents unintentional recognition of self-RNA. *Elife*, **4**, 1–20.
32. Fitzgerald,M.E., Rawling,D.C., Potapova,O., Ren,X., Kohlway,A. and Pyle,A.M. (2017) Selective RNA targeting and regulated signaling by RIG-I is controlled by coordination of RNA and ATP binding. *Nucleic Acids Res.*, **45**, 1442–1454.
33. Peisley,A., Lin,C., Wu,B., Orme-Johnson,M., Liu,M., Walz,T. and Hur,S. (2011) Cooperative assembly and dynamic disassembly of MDA5 filaments for viral dsRNA recognition. *Proc. Natl. Acad. Sci. U. S. A.*, **108**, 21010–21015.
34. Oda,H., Nakagawa,K., Abe,J., Awaya,T., Funabiki,M., Hijikata,A., Nishikomori,R., Funatsuka,M., Ohshima,Y., Sugawara,Y., *et al.* (2014) Aicardi-goutières syndrome is caused by IFIH1 mutations. *Am. J. Hum. Genet.*, **95**, 121–125.
35. Miner,J.J. and Diamond,M.S. (2014) MDA5 and autoimmune disease. *Nat. Genet.*, **46**, 418–419.
36. Jang,M.A., Kim,E.K., Now,H., Nguyen,N.T.H., Kim,W.J., Yoo,J.Y., Lee,J., Jeong,Y.M., Kim,C.H., Kim,O.H., *et al.* (2015) Mutations in DDX58, which encodes RIG-I, Cause atypical singleton-merten syndrome. *Am. J. Hum. Genet.*, **96**, 266–274.
37. Suthar,M.S., Ramos,H.J., Brassil,M.M., Netland,J., Chappell,C.P., Blahnik,G., McMillan,A., Diamond,M.S., Clark,E.A., Bevan,M.J., *et al.* (2012) The RIG-I-like Receptor LGP2 Controls CD8+ T Cell Survival and Fitness. *Immunity*, **37**, 235–248.
38. Widau,R.C., Parekh,A.D., Ranck,M.C., Golden,D.W., Kumar,K.A., Sood,R.F., Pitroda,S.P., Liao,Z., Huang,X., Darga,T.E., *et al.* (2014) RIG-I-like receptor LGP2 protects tumor cells from ionizing radiation. *Proc. Natl. Acad. Sci. U. S. A.*, **111**, 3–10.
39. Takahashi,T., Nakano,Y., Onomoto,K., Yoneyama,M. and Ui-Tei,K. (2020) LGP2 virus sensor enhances apoptosis by upregulating apoptosis regulatory genes through TRBP-bound miRNAs during viral infection. *Nucleic Acids Res.*, **48**, 1494–1507.

40. Baechler,E.C., Batliwalla,F.M., Karypis,G., Gaffney,P.M., Ortmann,W.A., Espe,K.J., Shark,K.B., Grande,W.J., Hughes,K.M., Kapur,V., *et al.* (2003) Interferon-inducible gene expression signature in peripheral blood cells of patients with severe lupus. *Proc. Natl. Acad. Sci. U. S. A.*, **100**, 2610–2615.
41. Banchereau,R., Hong,S., Cantarel,B., Baldwin,N., Baisch,J., Edens,M., Cepika,A.M., Acs,P., Turner,J., Anguiano,E., *et al.* (2016) Erratum: Personalized immunomonitoring uncovers molecular networks that stratify lupus patients ((Cell (2016) 165 (551-565)). *Cell*, **165**, 1548–1550.
42. Van Baarsen,L.G.M., Bos,W.H., Rustenburg,F., Van Der Pouw Kraan,T.C.T.M., Wolbink,G.J.J., Dijkmans,B.A.C., Van Schaardenburg,D. and Verweij,C.L. (2010) Gene expression profiling in autoantibody-positive patients with arthralgia predicts development of arthritis. *Arthritis Rheum.*, **62**, 694–704.
43. Tan,F.K., Zhou,X., Mayes,M.D., Gourh,P., Guo,X., Marcum,C., Jin,L. and Arnett,F.C. (2006) Signatures of differentially regulated interferon gene expression and vasculotrophism in the peripheral blood cells of systemic sclerosis patients. *Rheumatology*, **45**, 694–702.
44. Nestle,F.O., Conrad,C., Tun-Kyi,A., Homey,B., Gombert,M., Boyman,O., Burg,G., Liu,Y.J. and Gilliet,M. (2005) Plasmacytoid predendritic cells initiate psoriasis through interferon-α production. *J. Exp. Med.*, **202**, 135–143.
45. Rabinovitch,A. and Suarez-Pinzon,W.L. (2003) Role of Cytokines in the Pathogenesis of Autoimmune Diabetes Mellitus. *Rev. Endocr. Metab. Disord.*, **4**, 291–299.
46. Ruiz-Riol,M., Barnils,M. del P.A., Colobran Oriol,R., Pla,A.S., Borràs Serres,F.-E., Lucas-Martin,A., Martínez Cáceres,E.M. and Pujol-Borrell,R. (2011) Analysis of the cumulative changes in Graves' disease thyroid glands points to IFN signature, plasmacytoid DCs and alternatively activated macrophages as chronicity determining factors. *J. Autoimmun.*, **36**, 189—200.
47. Casrouge,A., Zhang,S.-Y., Eidenschenk,C., Jouanguy,E., Puel,A., Yang,K., Alcais,A., Picard,C., Mahfoufi,N., Nicolas,N., *et al.* (2006) Herpes Simplex Virus Encephalitis in Human UNC-93B Deficiency. *Science (80-.).*, **314**, 308 LP – 312.

48. Dupuis,S., Jouanguy,E., Al-Hajjar,S., Fieschi,C., Al-Mohsen,I.Z., Al-Jumaah,S., Yang,K., Chapgier,A., Eidenschenk,C., Eid,P., *et al.* (2003) Impaired response to interferon-alpha/beta and lethal viral disease in human STAT1 deficiency. *Nat. Genet.*, **33**, 388—391.
49. Minegishi,Y., Saito,M., Morio,T., Watanabe,K., Agematsu,K., Tsuchiya,S., Takada,H., Hara,T., Kawamura,N., Ariga,T., *et al.* (2006) Human Tyrosine Kinase 2 Deficiency Reveals Its Requisite Roles in Multiple Cytokine Signals Involved in Innate and Acquired Immunity. *Immunity*, **25**, 745–755.
50. Jouanguy,E., Zhang,S.-Y., Chapgier,A., Sancho-Shimizu,V., Puel,A., Picard,C., Boisson-Dupuis,S., Abel,L. and Casanova,J.-L. (2007) Human primary immunodeficiencies of type I interferons. *Biochimie*, **89**, 878—883.
51. Rice,G.I., Kasher,P.R., Forte,G.M.A., Mannion,N.M., Greenwood,S.M., Szynkiewicz,M., Dickerson,J.E., Bhaskar,S.S., Zampini,M., Briggs,T.A., *et al.* (2012) Mutations in ADAR1 cause Aicardi-Goutières syndrome associated with a type I interferon signature. *Nat. Genet.*, **44**, 1243–1248.
52. Li,Y., Banerjee,S., Goldstein,S.A., Dong,B., Gaughan,C., Rath,S., Donovan,J., Korennykh,A., Silverman,R.H. and Weiss,S.R. (2017) Ribonuclease l mediates the cell-lethal phenotype of double-stranded RNA editing enzyme ADAR1 deficiency in a human cell line. *Elife*, **6**, 1–18.
53. Malathi,K., Dong,B., Gale,M. and Silverman,R.H. (2007) Small self-RNA generated by RNase L amplifies antiviral innate immunity. *Nature*, **448**, 816–819.
54. Bonnevie-Nielsen,V., Field,L.L., Lu,S., Zheng,D.J., Li,M., Martensen,P.M., Nielsen,T.B., Beck-Nielsen,H., Lau,Y.L. and Pociot,F. (2005) Variation in antiviral 2′,5′-oligoadenylate synthetase (2′5′AS) enzyme activity is controlled by a single-nucleotide polymorphism at a splice-acceptor site in the OAS1 gene. *Am. J. Hum. Genet.*, **76**, 623–633.
55. Funabiki,M., Kato,H., Miyachi,Y., Toki,H., Motegi,H., Inoue,M., Minowa,O., Yoshida,A., Deguchi,K., Sato,H., *et al.* (2014) Autoimmune Disorders Associated with Gain of Function of the Intracellular Sensor MDA5. *Immunity*, **40**, 199–212.

56. Gack,M.U., Kirchhofer,A., Shin,Y.C., Inn,K.S., Liang,C., Cui,S., Myong,S., Ha,T., Hopfner,K.P. and Jung,J.U. (2008) Roles of RIG-I N-terminal tandem CARD and splice variant in TRIM25-mediated antiviral signal transduction. *Proc. Natl. Acad. Sci. U. S. A.*, **105**, 16743–16748.
57. Gack,M.U., Shin,Y.C., Joo,C.-H., Urano,T., Liang,C., Sun,L., Takeuchi,O., Akira,S., Chen,Z., Inoue,S., *et al.* (2007) TRIM25 RING-finger E3 ubiquitin ligase is essential for RIG-I-mediated antiviral activity. *Nature*, **446**, 916–920.
58. Jiang,X., Kinch,L.N., Brautigam,C.A., Chen,X., Du,F., Grishin,N. V. and Chen,Z.J. (2012) Ubiquitin-Induced Oligomerization of the RNA Sensors RIG-I and MDA5 Activates Antiviral Innate Immune Response. *Immunity*, **36**, 959–973.
59. Lang,X., Tang,T., Jin,T., Ding,C., Zhou,R. and Jiang,W. (2017) TRIM65-catalized ubiquitination is essential for MDA5-mediated antiviral innate immunity. *J. Exp. Med.*, **214**, 459–473.
60. Arimoto,K.I., Takahashi,H., Hishiki,T., Konishi,H., Fujita,T. and Shimotohno,K. (2007) Negative regulation of the RIG-I signaling by the ubiquitin ligase RNF125. *Proc. Natl. Acad. Sci. U. S. A.*, **104**, 7500–7505.
61. Onomoto,K., Jogi,M., Yoo,J.S., Narita,R., Morimoto,S., Takemura,A., Sambhara,S., Kawaguchi,A., Osari,S., Nagata,K., *et al.* (2012) Critical role of an antiviral stress granule containing RIG-I and PKR in viral detection and innate immunity. *PLoS One*, **7**.
62. Hajake,T., Matsuno,K., M. Kasumba,D., Oda,H., Kobayashi,M., Miyata,N., Shinji,M., Kogure,A., Kasajima,N., Okamatsu,M., *et al.* (2019) Broad and systemic immune-modulating capacity of plant-derived dsRNA. *Int. Immunol.*, 10.1093/intimm/dxz054.
63. Childs,K.S., Randall,R.E. and Goodbourn,S. (2013) LGP2 Plays a Critical Role in Sensitizing mda-5 to Activation by Double-Stranded RNA. *PLoS One*, **8**.
64. Berke,I.C., Yu,X., Modis,Y. and Egelman,E.H. (2012) MDA5 assembles into a polar helical filament on dsRNA. *Proc. Natl. Acad. Sci. U. S. A.*, **109**, 18437–18441.
65. Bruns,A.M., Leser,G.P., Lamb,R.A. and Horvath,C.M. (2014) The Innate Immune Sensor LGP2 Activates Antiviral Signaling by Regulating MDA5-RNA Interaction and Filament Assembly. *Mol. Cell*, **55**, 771–781.

66. Suzuki,Y., Gilmore,J.L., Yoshimura,S.H., Henderson,R.M., Lyubchenko,Y.L. and Takeyasu,K. (2011) Visual analysis of concerted cleavage by type IIF restriction enzyme SfiI in subsecond time region. *Biophys. J.*, **101**, 2992–2998.
67. Yokokawa,M., Wada,C., Ando,T., Sakai,N., Yagi,A., Yoshimura,S.H. and Takeyasu,K. (2006) Fast-scanning atomic force microscopy reveals the ATP/ADP-dependent conformational changes of GroEL. *EMBO J.*, **25**, 4567–4576.
68. Yoshimura,S.H., Ohniwa,R.L., Sato,M.H., Matsunaga,F., Kobayashi,G., Uga,H., Wada,C. and Takeyasu,K. (2000) DNA phase transition promoted by replication initiator. *Biochemistry*, **39**, 9139–9145.
69. Yu,Q., Qu,K. and Modis,Y. (2018) Cryo-EM Structures of MDA5-dsRNA Filaments at Different Stages of ATP Hydrolysis. *Mol. Cell*, **72**, 999-1012.e6.
70. Shah,N., Beckham,S.A., Wilce,J.A. and Wilce,M.C.J. (2018) Combined roles of ATP and small hairpin RNA in the activation of RIG-I revealed by solution-based analysis. *Nucleic Acids Res.*, **46**, 3169–3186.
71. Berke,I.C., Li,Y. and Modis,Y. (2013) Structural basis of innate immune recognition of viral RNA. *Cell. Microbiol.*, **15**, 386–394.
72. Patel,J.R., Jain,A., Chou,Y.Y., Baum,A., Ha,T. and García-Sastre,A. (2013) ATPase-driven oligomerization of RIG-I on RNA allows optimal activation of type-I interferon. *EMBO Rep.*, **14**, 780–787.
73. Parisien,J., Lenoir,J.J., Mandhana,R., Rodriguez,K.R., Qian,K., Bruns,A.M. and Horvath,C.M. (2018) RNA sensor LGP 2 inhibits TRAF ubiquitin ligase to negatively regulate innate immune signaling . *EMBO Rep.*, **19**.
74. Hikima,J. ichi, Yi,M.K., Ohtani,M., Jung,C.Y., Kim,Y.K., Mun,J.Y., Kim,Y.R., Takeyama,H., Aoki,T. and Jung,T.S. (2012) LGP2 Expression is Enhanced by Interferon Regulatory Factor 3 in Olive Flounder, Paralichthys olivaceus. *PLoS One*, **7**.

Chapter 6

Acknowledgement

I would like to thank the following people, without whom I would not be able to complete this research:

My supervisor, Prof. Takashi Fujita at Kyoto University, whose patience steered me through my work, thank you from the bottom of my heart.

Many thanks to Prof. Shige H. Yoshimura, who allowed me to use the AFM machine in his laboratory, and his students who offered help when I needed.

I would like to say a special thank you to the Prof. Hisashi Tadakuma at Osaka University and ShanghaiTech University who sacrificed his time and supported me through my research, as well as writing. Without your help and guidance this project would have not been the same.

My sincere gratitude to Prof. Yuki Suzuki, Ryo Yamaue and Katashi Deguchi for their help with AFM data.

To my husband – I simply couldn't have done this without you. Thank you for all your unconditional support through these very intense academic years, thank you for always encouraging me.

This work was supported by the research grants from the Ministry of Education, Culture, Sports, Science and Technology of Japan: Innovative Areas “Infection Competency” [grant number 24115004]; Japan Agency for Medical Research and Development: Research Program on Emerging and Re-emerging Infectious Diseases [grant number 19fk0108081h1001]; Japanese Society for the Promotion of Science: Core to Core Program: Grants-in-Aid for Scientific Research “B” [grant number 18H02344, 16KT0068 and 19H03197] and Grant-in-Aid for Scientific Research on Innovative Areas [grant number JP19H04830]; Fund for the Promotion of Joint International Research: Fostering Joint International Research (B) [grant number 18KK0232]; University of Bonn, ImmunoSensation [EXC2151-390873048]

This thesis is based on the material contained in the following scholarly paper:

Viral RNA recognition by LGP2 and MDA5, and activation of signaling through step-by-step conformational changes

Ivana Duic, Hisashi Tadakuma, Yoshie Harada, Ryo Yamaue, Katashi Deguchi, Yuki Suzuki, Shige H. Yoshimura, Hiroki Kato, Kunio Takeyasu and Takashi Fujita

Nucleic Acids Research, Oxford University Press, volume 48, issue 20, 18 November 2020, Pages 11664–11674

Published ahead of print: 02 November 2020

DOI: 10.1093/nar/gkaa935